

1 Late Holocene structural style and seismicity of highly 2 transpressional faults in southern Haiti

3 **Jiannan Wang, Paul Mann, Robert R. Stewart**

4 Department of Earth and Atmospheric Sciences, University of Houston, Houston, Texas, USA.

5 **Key Points:**

- 6 First high-resolution sonar surveys of two actively deforming lakes in Haiti.
- 7 High degree of regional, tectonic transpression is partitioned by *en echelon* thrust
8 faults and associated folds adjacent to a major strike-slip, plate boundary fault.
- 9 3D deformation model integrates patterns of 2010 coseismic uplift, aftershock dis-
10 tribution, and mapped geologic structures.

11 **Abstract**

12 The devastating 2010 Haiti earthquake (M_w 7.0) was caused by rupture of the Léogâne,
 13 blind, thrust fault located 5 km north of the 1200 km-long, left-lateral, Enriquillo-Plantain
 14 Garden fault zone (EPGFZ). Unexpectedly, the EPGFZ remained largely quiescent or
 15 slightly reactivated during the 2010 earthquake. However, the EPGFZ still formed a bound-
 16 ary between a coseismically uplifted lowland north of the EPGFZ and a subsided area
 17 in the highlands south of the fault. Here, we use high-resolution sonar data from two,
 18 Haitian lakes that straddle the EPGFZ and its northern flank to demonstrate the presence
 19 of a 10 – 15 km-wide, 120 km-long, late Holocene fold-thrust belt which deforms clas-
 20 tic, lowland basins along the northern edge of the EPGFZ. In the eastern part of the study
 21 area, sonar results from Lake Azuey show that the linear trace of the EPGFZ cutting the
 22 Holocene lake bed is more deeply buried and less active than the adjacent, newly discov-
 23 ered, northwest-striking, northeast-dipping Jimani thrust fault that is part of the adjacent
 24 transpressional belt of *en echelon* thrusts and folds. This structural relationship between a
 25 less active EPGFZ and more recently active, transpression-related Jimani thrust is remark-
 26 ably similar to the 2010 epicentral area 70 km to the west between the less active EPGFZ
 27 and seismogenic Léogâne thrust during the 2010 Haiti earthquake. In this complex trans-
 28 pressional zone, we propose that coseismic deformation alternates at recurrence intervals
 29 of centuries between oblique, transpression-related structures (Léogâne, Jimani, and Trois
 30 Baies thrusts) and the main strike-slip, plate boundary fault zone (EPGFZ).

31 **1 Introduction and tectonic setting of the 2010 Haiti earthquake**

32 On January 12, 2010, a M_w 7.0 earthquake struck the densely populated, greater
 33 Port-au-Prince region of south-central Haiti and caused widespread destruction with over
 34 230,000 fatalities and an estimated 10 billion dollars damage [Prentice *et al.*, 2010; Bil-
 35 ham, 2010; Paultre *et al.*, 2013; Kocel *et al.*, 2016] (Figure 1). Multidisciplinary, geolog-
 36 ical and geophysical studies about the 2010 epicentral area of south-central Haiti have
 37 been done, including: 1) coseismic, coral reef uplift observation along a 50 km-long area
 38 of coastline in the epicentral region combined with fault modeling [Hayes *et al.*, 2010];
 39 2) coseismic, vertical ground motion from radar interferometry [Hashimoto *et al.*, 2011];
 40 3) high-resolution, surface-fault-trace mapping using Light Detection And Ranging (LI-
 41 DAR) and targeted field studies [Cowgill *et al.*, 2012]; 4) Global Positioning System (GPS)
 42 and 2010 aftershock-based studies and modeling of pre-, syn-, and post-2010 earthquake

43 crustal motions [Calais *et al.*, 2010; Nettles and Hjörleifsdóttir, 2010; Symithe *et al.*, 2013;
44 Douilly *et al.*, 2013, 2015]; 5) ground-based studies of Holocene scarps including coseis-
45 mic ground fractures and late Quaternary scarps of the EPGFZ that remained unaffected
46 by 2010 fault breaks [Prentice *et al.*, 2010; Koehler and Mann, 2011; Rathje *et al.*, 2014;
47 Saint Fleur *et al.*, 2015]; 6) ground-based, near-surface, geophysical surveys of buried
48 faults activated during the 2010 earthquake [Kocel *et al.*, 2016]; 7) near-coast surveys of
49 submarine extensions of faults active in 2010 [Hornbach *et al.*, 2010; Mercier de Lépinay
50 *et al.*, 2011]; and 8) deepwater, marine surveys and coring to determine the recurrence in-
51 terval of major earthquakes based on anomalous sedimentary deposits related to shaking
52 and increased erosion [McHugh *et al.*, 2011]. The consensus from these previous, on- and
53 offshore, multidisciplinary studies is that the 2010 earthquake ruptured two, previously un-
54 recognized west- to northwest-striking thrust faults located 2 to 5 km north of the 1200
55 km-long, left-lateral, Enriquillo-Plantain Garden fault zone (EPGFZ) that forms a major,
56 plate boundary between the Caribbean plate to the south and the Gonâve microplate to the
57 north [Mann *et al.*, 1995; Calais *et al.*, 2010; Benford *et al.*, 2012; Corbeau *et al.*, 2016]
58 (Figure 1A, B). These two thrusts are separated by 6 km and include: 1) the subaerial, 8
59 km-long, blind, Léogâne thrust fault located 5 km north of the EPGFZ and trending at an
60 angle of 8° to the EPGFZ [Calais *et al.*, 2010; Douilly *et al.*, 2013, 2015]; and 2) the sub-
61 marine, 20 km-long Trois Baies thrust fault located 2 km north of the EPGFZ and trend-
62 ing at an angle of 20° [Mercier de Lépinay *et al.*, 2011; Symithe *et al.*, 2013] (Figure 1B,
63 C).

64 Despite the proximity of the Léogâne and Trois Baies thrust to the neighboring
65 EPGFZ, the EPGFZ remained largely quiescent and outside the zone of maximum, co-
66 seismic uplift and ground shaking and aftershocks related to the 2010 earthquake [Nettles
67 and Hjörleifsdóttir, 2010]. The centroid moment tensor (CMT) mechanism of the main
68 2010 shock shows a primarily strike-slip motion, with a small component of reverse mo-
69 tion, on a steeply north-dipping nodal plane [Nettles and Hjörleifsdóttir, 2010; Douilly
70 *et al.*, 2013]. Finite element modeling [Douilly *et al.*, 2015] suggests that Léogâne fault
71 buried beneath at least 1 km of overlying undeformed clastic sediment in the area north
72 of the EPGFZ absorbed most of the energy of the northeast-southwest compression along
73 obliquely-striking, high-angle (21°-70° dipping) reverse fault planes. For this reason, there
74 was insufficient stress to trigger slip during the 2010 earthquake on the EPGFZ 5 km to
75 the south (Figure 1B). Previous GPS surveys [Calais *et al.*, 2010, 2016] along this area of

76 the EPGFZ display vectors at almost right angles to these obliquely-striking thrusts and
 77 consistent with their preferred reactivation (Figure 1A, B).

78 Aftershock studies following the 2010 earthquake by *Douilly et al.* [2013, 2015]
 79 showed that the EPGFZ moved slightly at depth and acted as a 6 km-long, east-west and
 80 sub-vertical, connecting fault segment that transmitted seismogenic motion between the
 81 obliquely-trending, north-dipping, Léogâne fault in the east and the more obliquely-trending,
 82 southwest-dipping Trois Baies fault in the west (Figure 1B). However, post-earthquake ge-
 83 ologic reconnaissance revealed no surface ground breaks along the proposed onland areas
 84 of EPGFZ in the epicentral region of the earthquake [*Prentice et al.*, 2010; *Koehler and*
 85 *Mann*, 2011; *Rathje et al.*, 2014]. A more recent study by *Saint Fleur et al.* [2015] pro-
 86 posed previously, unrecognized, 2010 coseismic groundbreaks along the obliquely-trending
 87 Lamentin thrust 11 km east of the epicentral area near the city of Port-au-Prince (Figure
 88 2A).

89 *En echelon* thrusts spacing at distances of 1-8 km along the main strike-slip fault,
 90 obliquely intersect the main strike-slip fault at angles of 30° – 45°. These structures strike
 91 northwestward away from the EPGFZ with individual oblique, fault lengths extending into
 92 the deeper basins at distances of 4-29 km (Figure 2A). As a result of this distinctive and
 93 regular intersecting fault geometry between these oblique thrusts and the linear EPGFZ,
 94 earthquake rupture initiating on an oblique thrust, as seen for the Léogâne fault in 2010, is
 95 likely confined to that vicinity and may not connect with other oblique thrusts or even the
 96 EPGFZ itself [*Douilly et al.*, 2013, 2015].

97 Coseismic deformation along a large transpressional strike-slip fault, such as the
 98 EPGFZ [*Calais et al.*, 2002] in Hispaniola or the San Andreas fault zone in California
 99 [*Segall and Lisowski*, 1990], either is accommodated by slip and major earthquakes on
 100 the main, strike-slip plate boundary fault, or is accommodated by the oblique, *en echelon*
 101 thrusts adjacent to the main fault, or is accommodated by both sets of faults (cf. compila-
 102 tion of types of destructive earthquakes in transpressional settings by *Hayes et al.* [2010]).
 103 Motions on distributed, *en echelon* thrusts do not necessarily spare or reduce coseismic
 104 rupture on the main strike-slip fault because the *en echelon* and main strike-slip fault re-
 105 main separate fault planes, and the main strike-slip fault could continue to accumulate
 106 strain. In an extreme case, plate motions become increasingly transpressional as seen in
 107 the case of the EPGFZ as manifested in the obliquity of GPS vectors relative to the strike

108 of the EPGFZ (Figure 1A, B) or in a restraining bend setting or during the plate reorga-
 109 nizations. In these settings, the *en echelon*, oblique thrusts might assume more and more
 110 plate-edge strain to the point that the plate boundary behaves more like a broad, thrust
 111 boundary and less like a narrow, strike-slip boundary.

112 These oblique and *en echelon* thrust faults in transpressional settings, including large
 113 restraining bends as in Hispaniola, potentially nucleate “uncharacteristic earthquakes” of
 114 varying recurrence intervals and sizes that are distinct from the recurrence intervals and
 115 sizes of the adjacent but independent strike-slip fault [Fielding *et al.*, 2013]. Restraining
 116 bend areas like Hispaniola can lead to the generation and increased activities on more
 117 favorably and obliquely oriented folds and thrusts whose coseismic rupture might alter-
 118 nate with much longer ruptures along the adjacent strike-slip fault. The number of these
 119 *en echelon* thrust faults, in restraining bend setting, can be large at observed spacings of
 120 5-10 km dispersed along the trend of strike-slip faults that may be hundreds of kilometers
 121 in total length. For this reason, the identification of oblique *en echelon* thrusts, especially
 122 when buried or “blind”, can be challenging, assessing their role with seismogenesis within
 123 a broad plate boundary [Frankel *et al.*, 2011].

124 2 Objectives and methods

125 2.1 Study area

126 This elongate, belt of transpressional deformation associated with *en echelon* thrusts
 127 occupies a topographically-low, densely populated Cul-de-Sac basin underlain by poorly
 128 consolidated clastic sedimentary rocks ranging in age from Miocene to Recent [Mas-
 129 soni, 1955; Mann *et al.*, 1995; Terrier *et al.*, 2014; Saint Fleur *et al.*, 2015]. In easternmost
 130 Haiti, this belt is overlain by the shallow (33 m-deep), 138 km², brackish Lake Azuey
 131 near the border separating Haiti from the Dominican Republic [Wright *et al.*, 2015; Pi-
 132 asecki *et al.*, 2016]. Lake Enriquillo to the east is a larger, shallow (52 m-deep), 346 km²,
 133 hypersaline, sub-sealevel lake located entirely in the Dominican Republic and separated
 134 from Lake Azuey by the eastward continuation of the same transpressional belt parallel
 135 and north of the EPGFZ in the Cul-de-Sac valley [Mann *et al.*, 1995] (Figure 1B).

136 In the western part of our study area, the more transtensional segment of the EPGFZ
 137 is overlain by the 42.8 m-deep, 14 km², freshwater Lake Miragoâne (Figure 1B). All
 138 three of these shallow, inland, lakes experience variations up to 13 m in their surface el-

139 evations due to annual to decadal changes in climate and rainfall amounts including ex-
 140 treme rainfall associated with hurricanes [Wright *et al.*, 2015; Piasecki *et al.*, 2016; Mokna-
 141 tian *et al.*, 2017; Rico, 2017].

142 2.2 Objectives

143 The main goal of this paper are to better integrate the geologic structure of the
 144 120 km-long study area, which parallels the trace of the EPGFZ and includes the 2010
 145 epicentral area, using a wealth of geologic, geophysics, GPS, radar interferometry, af-
 146 tershock, and modeling studies, most of which has been collected since the 2010 earth-
 147 quake. Our primary objective is to use these information to structurally characterize the
 148 10-15 km-wide, belt of late Holocene, transpressional deformation that forms a laterally-
 149 extensive, deformed belt along the inland, Cul-de-Sac intermontane basin in the east and
 150 the low-relief coastal plain along Port-au-Prince bay and the Canal du Sud to the west
 151 (Figure 1B). In particular, we focus on the identifying a family of *en echelon* thrusts, whose
 152 curvilinear strikes area are very similar to the Léogâne thrust now known to be responsi-
 153 ble for most of the energy release and coseismic uplift during the 2010 Haiti earthquake
 154 [Calais *et al.*, 2010; Douilly *et al.*, 2013, 2015] (Figure 1B, Figure 2A).

155 2.3 Survey design

156 In order to understand the geologic and structural styles of transpression within this
 157 belt, including the age relations between deformation in the north-flanking belt and the
 158 EPGFZ itself, we collected a total of 94 km of high-resolution (2-10 kHz) sonar profiles
 159 in 2014 from the 138 km², brackish Lake Azuey and 37 km of profiles from the 14 km²,
 160 fresh-water Lake Miragoâne (Figure 1B). The EPGFZ strikes through both of the lakes,
 161 so 80% of our lines on Lake Azuey and 90% of our survey lines on Lake Miragoâne was
 162 dedicated to the across fault-strike, north-south profiles.

163 The average speed of the boat towing the sonar was 3 knots, and we used a sonar
 164 pulse rate of 4 per second. Our 2-10 kHz sonar frequency range gives sub-bottom layer
 165 resolution of about 10 cm. These surveys were the first sonar surveys in Haitian lakes.
 166 Both lakes straddle the projected active trace of Haiti's EPGFZ and its adjacent, transpres-
 167 sional fold-thrust belt, therefore provide new constraints on the location, structural style,
 168 and timing of deformation within both structural provinces. We incorporate these lake

169 data with previous geologic mapping, geophysical observations related to the 2010 earth-
 170 quake, and regional information on plate motions in this region (Figure 1B).

171 **3 Tectonic setting of transpressional deformation in south-central Haiti including
 172 unresolved tectonic and structural questions**

173 **3.1 Previous strike-slip deformational model vs. Haiti thrust belt deformational
 174 model**

175 There are two regional structural models to explain the present-day structure of the
 176 broad, 250 km-wide zone of transpression spanning the entire width of the island of His-
 177 paniola.

178 **3.1.1 Strike-slip, regional structural model**

179 The first is the strike-slip-dominated model, driven by oblique motion and transpres-
 180 sion between the thick and buoyant Bahamas platform on the North America plate, the
 181 Caribbean plate, and the Gonâve microplate [Mann *et al.*, 1995; Dolan *et al.*, 1998; Mann
 182 *et al.*, 2002; Calais *et al.*, 2002, 2016] (Figure 1A, B). Structures and tectonic geomor-
 183 phology formed in this 250 km-wide, transpressional zone include: GPS studies [Calais
 184 *et al.*, 2002, 2010; Hayes *et al.*, 2010; Symithe *et al.*, 2013; Douilly *et al.*, 2013, 2015] re-
 185 veal strain partitioning along the EPGFZ and the subparallel Septentrional strike-slip fault
 186 zone (which is the plate boundary between North Hispaniola microplate and Gonâve mi-
 187 croplate) (Figure 1A). As a result of transpression, the central Hispaniola has the highest
 188 topography, up to 3 km, in all of the northern Caribbean region. The left-lateral strike-
 189 slip rupture of the EPGFZ in the 18th century inferred from historical earthquakes [Bakun
 190 *et al.*, 2012] with average left-lateral offset amounts of 1.3 – 3.3 m as expressed along off-
 191 set streams of the EPGFZ [Prentice *et al.*, 2010] and by left-lateral, channel offsets of 7 –
 192 8 m along stream channels by the Septentrional fault zone [Prentice *et al.*, 1993; Leroy
 193 *et al.*, 2015]. Saint Fleur *et al.* [2015]’s study indicates the folding and thrusting of 10
 194 – 15 km-wide belt of Miocene to Quaternary rock adjacent to the EPGFZ. In addition,
 195 Mann *et al.* [2002]; Grindlay *et al.* [2005]; Kroehler *et al.* [2011] suggest a strong, south-
 196 westward, backthrusting of the Gonâve microplate, in southern Hispaniola in Haiti and
 197 Dominican Republic to the southwest onto the Caribbean plate (Figure 1B, C). Southwest-
 198 ward backthrusting of Hispaniola is manifested by the accretionary wedges present along
 199 the Muerto trench south of the Dominican Republic [Bien-Aimé Momplaisir, 1986; Bruña

200 *et al.*, 2009] (Figure 1B) and along the southern margin of Haiti (South Haiti accretionary
 201 prism [Bien-Aimé Momplaisir, 1986] (Figure 1C), along with the associated, localized,
 202 negative gravity anomaly associated with plate flexure under a thrust load [Mann *et al.*,
 203 2002; Bruña *et al.*, 2009] (Figure 1A)).

204 ***3.1.2 Criticisms of the strike-slip, regional structural model***

205 Two criticisms have been proposed for the strike-slip model. First, Corbeau *et al.*
 206 [2016] has questioned whether the predictions of the GPS-based block models, which pre-
 207 dict significant shortening, are accurate in that little transpression-related shortening can
 208 be observed from regional seismic profiles in the offshore area of the Gulf of Gonâve
 209 north of the southern peninsula of Haiti, or in the area of the Jamaica Passage east of
 210 Haiti. Second, Symithe and Calais [2016] have proposed that there is no geologic evi-
 211 dence for a continuation of the EPGFZ east of latitude 72.27°W in the eastern Cul-de-Sac
 212 Valley, Lake Azuey and Lake Enriquillo in the Dominican Republic (Figure 1B). Instead,
 213 Symithe and Calais [2016] propose that large rates of north-south shortening predicted
 214 from GPS block models is taken up entirely by low-angle thrust structures in the east-
 215 ern Cul-de-Sac and Enriquillo Valleys that were modeled using GPS data as part of their
 216 study.

217 ***3.1.3 Trans-Haitian fold-and-thrust belt regional structural model***

218 The Trans-Haitian fold-and-thrust belt model originated with a study by Pubellier
 219 *et al.* [2000], who proposed a low-angle southwestward-verging fold-and-thrust belt along
 220 the southwestern edge of the central Hispaniola block. The thrust front of this feature was
 221 thought to be actively propagating from the main Trans-Haitian fold-and-thrust belt, lo-
 222 cated in the Chaîne des Matheux (Figure 1B, Figure 2A), southwestward into the area of
 223 the Léogâne plain and the Cul-de-Sac basin (Figure 2A, B). Pubellier *et al.* [2000] pro-
 224 posed that the EPGFZ originally formed as a left-lateral strike-slip fault, but became inac-
 225 tive in the late Miocene when deformation in southern Hispaniola became compressional
 226 and the Trans-Haitian fold-and-thrust belt had propagated into the southern area of the
 227 Cul-de-Sac basin and Léogâne plain, where it emerged or “daylighted” to form the *en ech-*
 228 *elon*, convergent structures (compiled on the map in Figure 2). Pubellier *et al.* [2000] also
 229 proposed that the EPGFZ was reactivated as a normal fault in the Quaternary as a result

230 of crustal loading of the southern, foreland area by the overthrusting Trans-Haitian fold-
231 and-thrust belt.

232 Following the 2010 earthquake and the recognition of the north-dipping blind Léogâne
233 thrust fault, *Calais et al.* [2010] proposed that this fault is the leading edge of the Trans-
234 Haitian fold-and-thrust belt rather than being an *en echelon* thrust genetically linked to the
235 EPGFZ. In the interpretation proposed by *Calais et al.* [2010], the northward dip of the
236 Léogâne thrust made it difficult to link its origin with the EPGFZ, whose dip had been es-
237 tablished in this area as a vertical to high angle ($> 60^\circ$), south-dipping fault plane with ev-
238 idence of late Holocene, left-lateral offsets of drainages [*Prentice et al.*, 2010]. Moreover,
239 *Symithe and Calais* [2016] noted that Trans-Haitian fold-and-thrust belt regional model of
240 *Pubellier et al.* [2000] was more consistent with an increasing amount of GPS data sup-
241 portive of a larger magnitude, north-south shortening in central Hispaniola than with the
242 existence of an eastward extension of the left-lateral EPGFZ into the eastern part of Haiti
243 and the Dominican Republic (Figure 1B and Figure 2A).

244 **3.1.4 Criticisms of the Trans-Haitian fold-and-thrust belt, regional structural model**

245 First, *Mercier de Lépinay et al.* [2011] pointed out two problems with linking the
246 origin of the Léogâne thrust to the southwestward-propagating edge of the Trans-Haitian
247 fold-and-thrust belt: 1) the dip of the fault generating the main thrust, derived by *Mercier de*
248 *Lépinay et al.* [2011], was more steeply dipping (64°) than expected for a blind thrust at
249 the leading edge of a fold-thrust belt; and 2) the orientation of the N84°E fault plane of
250 the main shock is significantly oblique to the N120°E-oriented leading edge of the Trans-
251 Haitian fold-and-thrust belt as proposed by *Pubellier et al.* [2000]. In this paper, we dis-
252 cuss other inconsistencies with the zone of deformation north of the EPGFZ being the
253 result of southwestward propagation of the Trans-Haitian fold-and-thrust belt.

254 **4 New observations of the Late Holocene structural style along EPGFZ in southern 255 Haiti**

256 **4.1 Significance of *en echelon* thrusting and folding north and south of the EPGFZ**

257 The presence of a strike-slip fault at any scale is indicated by the presence of *en ech-*
258 *elon* arrays of thrust faults, normal faults, folds, fractures, dikes, and other linear features
259 in narrow, elongate zones [*Sylvester*, 1988]. On Figure 2A, we have compiled geologic in-

formation on *en echelon* folds and faults in a 10 – 15 km-wide zone of deformation along both the northern and southern flanks of the EPGFZ. Folds form as fault propagation folds along oblique, thrust faults, vary from 1 to 8 km in lateral spacing; and deform Miocene and younger fine to coarse-grained, basinal, and coastal plain rocks in the belt that is 10 – 15 km wide and extends parallel to the EPGFZ for 120 km (Figure 1B and Figure 2A). Folds in Neogene clastic lithologies of the Cul-de-Sac basin contrast with more continuous and longer wavelength, *en echelon* fold axes present in more massively-bedded Cretaceous to Eocene rigid, basaltic, and carbonate lithologies exposed in the 2 km-high range south of the EPGFZ, the Massif de Selle (Figure 2A). The trend of fold axes is similar to the north and south of the EPGFZ (Figure 2B).

The *en echelon* distribution of complex Holocene folding and thrusting in the 10 – 15 km wide zone of deformation north of the EPGFZ is also reflected in the complex pattern of 2010 coseismic and vertical deformation recorded by the interferogram from the 2010 epicentral area on the Léogâne plain west of the Cul-de-Sac basin [Hayes *et al.*, 2010; Hashimoto *et al.*, 2011; Bilham and Fielding, 2013] (Figure 2A). Douilly *et al.* [2013, 2015] and Kocel *et al.* [2016] use aftershocks and shallow geophysics to show that the 2010 Léogâne thrust fault and sub-parallel faults are overlain by at least one kilometer of undeformed and sub-horizontal strata.

4.2 Significance of curvilinear fold and thrust patterns in the transpressional belt north of the EPGFZ

The shaded relief DEM (digital elevation model) shown in Figure 2B reveals the curvilinear, *en echelon* fold morphologies that are defined by low, bedrock hills of Neogene sedimentary rocks exposed on the flat-lying Cul-de-Sac basin. These curvilinear fold axes can be related directly to a broad zone of left-lateral, simple shear produced along the sub-vertical and left-lateral EPGFZ based on several, basic observations seen on Figure 2B. The most prominent folds are present along the southern edge of the Cul-de-Sac basin within 15 km of the EPGFZ. In contrast, the central and northern edges of the Cul-de-Sac basin exhibit no prominent folding even directly adjacent to the base of Eocene-Miocene carbonate rocks forming the range [Pubellier *et al.*, 2000] (Figure 2A). The map-view shapes of fold axes along the southern margin of the Cul-de-Sac basin are asymptotic, or gently curve into east-west parallelism with the main trace of the EPGFZ along the southern edge of the Cul-de-Sac basin, as broad zones of shearing of thick, sed-

imentary basins (see the inset of Figure 2B; modified from *Odonne and Vialon* [1983]). Deeper, structural depressions form in the zone of convergent intersection between the east-west-striking EPGFZ and the northwest-striking, secondary thrusts as seen in the southern part of Lake Azuey, where the lake bends from an east-west trend adjacent to the EPGFZ to a more northwest trend in the central and northern part of the basin (Figure 2A, B).

298 **4.3 Geologic structure of the area of *en echelon* thrusts in the epicentral area on 299 the Léogâne fan-delta**

300 **4.3.1 Geologic structure of the Léogâne fan area**

301 A cross-sectional profile of the 2010 epicentral area related to the activation of two
302 conjugate thrust faults was modified from aftershock data from *Douilly et al.* [2013, 2015]
303 is shown in Figure 3 (Line A–A'). Both faults are buried by about 1 km of late Quater-
304 nary sand and gravel of the Léogâne fan delta [*Kocel et al.*, 2016] and an additional 1
305 km of Paleocene limestone. Aftershocks indicate that the main thrust event ruptured a
306 depth range of from 4 to 17 km beneath the ground surface [*Douilly et al.*, 2013, 2015].
307 The orientation of the Léogâne thrust based on gravity and uplift of coastal features is
308 east-west and parallel to recent near-surface breaks of the EPGFZ mapped in the shallow,
309 coastal zone adjacent to the Léogâne plain [*Hornbach et al.*, 2010]. Due to its proxim-
310 ity to the EPGFZ, an east-west strike of the Léogâne thrust is predicted as this is the area
311 where *en echelon* folds and faults curve into an asymptotic orientation relative to the main
312 EPGFZ, as shown on Figure 2B.

313 A radar interferogram compiled on the structure map of Figure 2A revealed that the
314 2010 earthquake elevated the smaller folds of the Léogâne fan-delta north of the EPGFZ,
315 yet produced coseismic subsidence in the 1.4 km-high, less complexly deformed, moun-
316 tain range south of the EPGFZ [*Hashimoto et al.*, 2011] (Figure 2A). This paradox can be
317 simply explained by the northward dip of the seismogenic Léogâne fault that elevated the
318 basinal area to the north (hanging wall of the Léogâne fault) and depressed the mountain-
319 ous area to the south (footwall block of the Léogâne fault (line A–A' in Figure 3).

320 **4.3.2 Geologic structure of the Port-au-Prince urban area compared to the Léogâne**
 321 **epicentral area**

322 A similar pattern of deformation is observed in Port-au-Prince urban area where the
 323 central and northern edge of the Cul-de-Sac basin is almost undeformed [Massoni, 1955;
 324 Cox *et al.*, 2011; McHugh *et al.*, 2011; Saint Fleur *et al.*, 2015] (Line B-B' in Figure 3).
 325 The cross section taken from workers, who were mapping 60 years ago when the city
 326 was smaller and the geology was less obscured by urbanization, shows two large thrusts, a
 327 range-bounding thrust along the southern edge of the city, and a northeast-dipping thrust,
 328 the Dumay thrust, that elevates a broad outcrop zone of north-dipping, Neogene sedimen-
 329 tary rocks on which the northern part of the city is built [Rathje *et al.*, 2014]. The 50°
 330 northeast dip of the Dumay thrust is similar to the 70° northeast dip of the Léogâne thrust
 331 to the west known from aftershocks [Douilly *et al.*, 2013, 2015], although the dip of the
 332 Dumay thrust reverses to a southwest dip as it approaches the EPGFZ (Figure 2A, B). On
 333 the cross section B-B' in Figure 3, we have schematically indicated areas that are elevated
 334 as a result of the northward dip of the Dumay thrust and the depression of the area to the
 335 south of the EPGFZ in the highlands south of the EPGFZ. If a future earthquake occurred
 336 along the north-dipping, *en echelon* thrust faults in the Port-au-Prince area (Line B-B' in
 337 Figure 3) or Lake Azuey area (Line C-C' in Figure 3) a similar uplift phenomenon proba-
 338 bly would occur where the lowlands are uplifted and the adjacent mountains subside.

339 **4.3.3 Geologic structure of the Lake Azuey area**

340 In the Lake Azuey area, we mapped a linear and east-west striking fault trace in
 341 deformed Holocene sediments along the projected trend of the landward traces of the
 342 EPGFZ both east and west of Lake Azuey (Figure 5 and Figure 6A, B). Integrated with
 343 previous land mapping of the EPGFZ [Bourgueil *et al.*, 1988; Mann *et al.*, 1995; Pren-
 344 tice *et al.*, 2010; Cowgill *et al.*, 2012], we interpret this linear east-west striking feature
 345 in Lake Azuey as a 5 m-wide and continuous trace of the EPGFZ which we can follow
 346 westward to the EPGFZ locality at Dumay, about half way between Lake Azuey and Port-
 347 au-Prince, which was previously described and dated as a 6 m-long, left-lateral offset of
 348 a late Holocene stream channel [Cowgill *et al.*, 2012] (locates at red circle, which is la-
 349 beled as Dumay in Figure 2A). The structural cross sections in this area taken from the
 350 previous studies [Massoni, 1955; Mann *et al.*, 1995; Douilly *et al.*, 2015] indicate that the
 351 high-angle EPGFZ co-exists with the adjacent thrusts that over-thrust from the south and

352 north (Line B–B' in Figure 3). We project this trace of the EPGFZ along a prominent
 353 fault valley at the town of Jimani that separates Lakes Azuey and Enriquillo (Figure 2A
 354 and Figure 5). Sonar profiles (Figure 6A, B) show that the most recent rupture of the
 355 EPGFZ is covered by about 0.7 m of Holocene sediment, suggesting that there has been
 356 late Holocene activity of the EPGFZ along the southern edge of the lake.

357 From sonar data, we observed late Holocene lake sediments onlapping onto local
 358 highs of Eocene limestone of the bounding range along the northern edge of the EPGFZ
 359 (Figure 6). The sonar from southern Lake Azuey suggests that the most prominent folds
 360 present adjacent to the EPGFZ become less prominent in the central and northern parts of
 361 the lake (Figure 2B). These southern folds and thrusts imaged in Lake Azuey define the
 362 transpressive belt along the EPGFZ observed in onshore areas to the west. On the cross
 363 section in Figure 6C, we have schematically indicated areas that are elevated as a result of
 364 the northward dip of the Jimani thrust and the depression of the area to the south of the
 365 EPGFZ.

366 The structural cross-section (Figure 6C) of the Lake Azuey area and the previous
 367 works [Massoni, 1955; Bourgueil *et al.*, 1988; Cox *et al.*, 2011; Douilly *et al.*, 2015] (Line
 368 A–A' and B–B' in Figure 3) along this 120 km-long zone of deformation adjacent to the
 369 EPGFZ show that the oblique thrust faults share a similar orientation with other northeast-
 370 dipping thrusts along the northern edge of the EPGFZ. All three of these oblique thrust
 371 faults (the Léogâne thrust in Line A–A', the Dumay thrust in Line B–B', and the Jimani
 372 thrust in Figure 6C) shown on the cross sections deform rocks as young as Pliocene and
 373 Quaternary [Saint Fleur *et al.*, 2015].

374 On a more regional scale, these observations form Lake Azuey are consistent with
 375 the multi-channel seismic reflection profile (named as Canadian Superior 2D and shown
 376 in Figure 1C), that shows a lack of intensive deformation in the part of Port-au-Prince
 377 Bay, that is the offshore, largely un-faulted and folded seaward extension of the Cul-de-
 378 Sac basin [McHugh *et al.*, 2011]. Pubellier *et al.* [2000] proposes that the Trans-Haitian
 379 fold-and-thrust belt exposed in the Chaine des Matheux range extends beneath the entire
 380 Cul-de-Sac and Port-au-Prince basins (Figure 2A, B). In summary, our observations at this
 381 scale do not support the previous model by Pubellier *et al.* [2000] and Calais *et al.* [2010]
 382 that folds and faults of the northern range are propagating southwestward beneath the zone
 383 of *en echelon* faults and folds (Figure 2A, B).

384 **4.4 Subsurface stratigraphy of Lake Azuey and Lake Enriquillo and paleoseis-**
 385 **mic estimates of the relative timing of recent earthquakes on the EPGFZ and**
 386 **secondary, *en echelon* thrust faults**

387 Our objective is to determine the relative age of the EPGFZ and its adjacent zone
 388 of fold-and-thrust deformation using the sonar profiles from Lakes Azuey and Enriquillo
 389 (Figure 4A). Previous coring, both in Lake Enriquillo [Rios *et al.*, 2013] (which was tied
 390 to the onshore stratigraphic studies [Taylor *et al.*, 1985; Rios *et al.*, 2013]) and in Lake
 391 Miragoâne [Higuera-Gundy *et al.*, 1999], has established the late Holocene 5 m and 7 m
 392 sedimentary history, respectively.

393 In Lake Enriquillo, a sonar survey similar to ours was conducted in 2013 [Rios
 394 *et al.*, 2013]. Mapping in both lakes revealed the presence of the east-west strands of
 395 the EPGFZ that are collinear with onshore scarps both east and west of Lake Azuey (Fig-
 396 ure 2, Figure 4, and Figure 5) and east and west of Lake Enriquillo [Mann *et al.*, 1995;
 397 Rios *et al.*, 2013]. These east-west fault strands abruptly truncate the trends of folds in
 398 the ranges south of the lake (Figure 5). The sonar events, which are interpreted as strati-
 399 graphic features, from Lake Azuey and Lake Enriquillo (Line B1 and Line L19 correlate
 400 convincingly (Figure 4B). Given the small distance separating the two lakes (about 4 km);
 401 the similarity of the stratigraphic profiles; and the same amount of sediment above the
 402 EPGFZ; it is reasonable to suggest that Lake Azuey and Lake Enriquillo share the same
 403 sedimentation history as well as the same structural style and seismicity related to the
 404 EPGFZ and its oblique, thrust faults.

405 The EPGFZ in both Lake Enriquillo and Lake Azuey is buried by 0.7 m of sedi-
 406 ments. According to coring studies in the Dominican Republic [Taylor *et al.*, 1985; Rios
 407 *et al.*, 2013], the 5.2 m thickness of the latest lake stage (2 ka BP to present) gives a re-
 408 cent Holocene average sedimentation rate of 2.6 mm/yr (Figure 4B). Using the average
 409 sediment rate, the most recent rupture of the EPGFZ would be dated to some 270 years
 410 ago. Given the historical earthquake records [Bakun *et al.*, 2012], we suggest that the most
 411 recent rupture of the EPGFZ corresponds to the historical events of October or November
 412 1751, and the deformed sediments in Lake Azuey are of Holocene age.

413 **4.5 Easternmost extent of the EPGFZ trace in Lake Enriquillo, Dominican Re-**
 414 **public**

415 Based on both of our lake surveys combined with a previous survey of Lake En-
 416 riquillo in the Dominican Republic [Rios *et al.*, 2013], and the previous geologic map-
 417 ping of the basinal and topographic corridor of the Cul-de-Sac basin in Haiti and the En-
 418 riquillo basin in the Dominican Republic [Mann *et al.*, 1995; Mann, 1999], a first-order
 419 question we pose is whether the EPGFZ extends as a continuous, strike-slip fault along
 420 the 120 km-long zone of deformation of Miocene and younger clastic rocks present be-
 421 tween the two lakes (Figure 1B and Figure 4A). The previous studies [Saint Fleur *et al.*,
 422 2015; Symithe and Calais, 2016] have proposed that the EPGFZ terminates as a strike-slip
 423 feature in the area south of Port-au-Prince. These studies further have proposed that trans-
 424 pressional plate motion in the eastern Cul-de-Sac basin and the Enriquillo Valley in the
 425 Dominican Republic (Figure 1B and Figure 4A) is entirely accommodated along the low-
 426 angle oblique-thrust structures that overthrust the southern edges of Lake Azuey and Lake
 427 Enriquillo.

428 A previous study of Lake Enriquillo by Rios *et al.* [2013] identified the break along
 429 the northeastern edge of Cabritos Island in Lake Enriquillo, which aligns exactly with the
 430 large east-western lineament extending eastward from our map area in Lake Azuey (Fig-
 431 ure 4A). The sonar results from both lakes show that the EPGFZ extends to at least to the
 432 eastern tip of Cabritos Island in the center of Lake Enriquillo, Dominican Republic (Fig-
 433 ure 4A). This survey revealed a fault penetrating the youngest sediment layer of Holocene
 434 age which is consistent with recent activity on this segment of the EPGFZ (Figure 6A, B).
 435 Therefore, we conclude that this linear, late Holocene strike-slip fault extends at 55 km
 436 (at least) to the eastern edge of Lake Enriquillo, where the previously documented [Mann
 437 *et al.*, 1995] uplift of the Holocene reef fringes Lake Enriquillo.

438 **5 Active tectonics of the area west of the 2010 epicentral zone in the western study**
 439 **area: Léogâne plain, Miragoâne basin, and their adjacent offshore area**

440 **5.1 The Trois Baies thrust fault, Canal du Sud, as the termination structure for**
 441 **the 2010 earthquake**

442 The 2010 aftershock zone at the western and central part of our study area (Fig-
 443 ure 7A) reflects the rupture along the northwest-striking, 20 km-long, submarine, Trois

444 Baies thrust fault that forms the western extension of the 10 – 15 km-wide, transpressional
 445 zone north of the EPGFZ. As the Trois Baies fault is submarine, InSAR cannot be used
 446 to assess its 2010 coseismic similarity with folding and thrusting along the Léogâne thrust
 447 that affected the onshore, Léogâne plain (Figure 7A).

448 However, the same basic structural elements of the Léogâne plain are also observed
 449 for the Trois Baies thrust fault, which include the short distance (1 km) to the EPGFZ and
 450 its steep (45°) but opposite (southwest) dip of the Trois Baies thrust fault (Figure 7). One
 451 of the most intense zones of coseismic, aftershock, coastal uplift [Hashimoto *et al.*, 2011],
 452 and subsidence [Prentice *et al.*, 2010] separates the oppositely-dipping Léogâne and Trois
 453 Baies faults, and may represent complex deformation at a transfer zone between the two
 454 faults (Figure 7A, B). The aftershock study of the Trois Baies fault [Symithe and Calais,
 455 2016] shows that its thrust character and oblique orientation in map view with the main
 456 EPGFZ is comparable to the cross sections of the eastern area in Figure 3. In the map
 457 view, the overall structure of this western part of the study area mirrors the same geomet-
 458rical relationship between the oblique thrusts (such as the Trois Baies thrust fault) and the
 459 main EPGFZ as described at the eastern part of the study area (Figure 2).

460 5.2 Structure of the Miragoâne pull-apart basin

461 In the onshore part of the western study area, Lake Miragoâne was interpreted as a
 462 14 km² pull-part basin developed as a left-stepping, releasing bend on the EPGFZ paired
 463 with the adjacent Tapion du Petit Goâve restraining bend 12 km to the east (Figure 7)
 464 [Cowgill *et al.*, 2012]. Bathymetry from our sonar data shows the maximum water depth
 465 of Lake Miragoâne is 42.8 m (Figure 7B), which makes this lake the deepest [Higuera-
 466 Gundy *et al.*, 1999] in the Caribbean region. The 30 m of recognizable stratigraphy (Fig-
 467 ure 8B and C) from the sonar survey in Lake Miragoâne reveals a series of deformational
 468 features including major east-west normal faults, minor thrust faults at depth (some 20 m),
 469 and active folds at the lake bottom (Figure 8). The upper 7 m of the lake sediments were
 470 cored and dated at 10 ka at the bottom of the core [Higuera-Gundy *et al.*, 1999]. By ap-
 471 plying the average sedimentary rate from the core data to the chirp sonar trace, we can
 472 extrapolate the sedimentation rate to the observed thickness of 30 m in the lake and esti-
 473 mate a minimum of 43 ka for the age of the pull-apart basin on the EPGFZ. Core mea-
 474 surements of the E/P (evaporation and precipitation ratio from the $\delta^{18}\text{O}$ of ostracod shells
 475 in the core sample) were undertaken [Higuera-Gundy *et al.*, 1999] in the center of Lake

476 Miragoâne (Figure 9B). The core reveals that the uppermost part of the sediments are
 477 Holocene to the latest Pleistocene in age (Figure 9A). Pollen data from the core indicate
 478 alternating dry and wet environments.

479 **5.3 Ages and sedimentary cycles of the Miragoâne pull-apart basin**

480 We applied a low-pass filter on the pollen log data (from the core acquired by *Higuera-*
 481 *Gundy et al.* [1999] in the center of the lake) and found a strong correlation between the
 482 pollen and sonar data (red curve in Figure 9B). To further investigate this interesting cor-
 483 relation between the geochemical and geophysical data, we use the filtered E/P log, con-
 484 sidered as pseudo-acoustic impedance log, to generate a synthetic sonar response (Fig-
 485 ure 9B). The correlation is compelling which suggests that the depositional environment
 486 influences the acoustic properties of the sediments and sonar response may be a partial
 487 proxy for climatic processes. In another words, the sediment layers from drier climates
 488 (higher E/P) have stronger acoustic reflectivity and vice versa. Combining the correlation
 489 between the pollen log and the acoustic reflections from the chirp sonar data, we can ex-
 490 tend the sedimentary history of the upper 7 m from the log data to the entire sonar data
 491 set. In the sonar profile, we find the most recent rupture in the lake is buried by about 0.5
 492 meter sediment (Figure 8B, C). The core dating result from *Higuera-Gundy et al.* [1999]
 493 suggests the age of these rupture is about 300 years old. The historical document record
 494 [*Bakun et al.*, 2012] indicates a historical earthquake happened in this area in 1770. Con-
 495 sidering the historical document record [*Bakun et al.*, 2012], the dating of the core, and
 496 the sonar interpretation in Lake Miragoâne suggest that the most recent rupture in this
 497 lake is likely related to the historic earthquake in 1770 [*Bakun et al.*, 2012].

498 **6 Discussion**

499 **6.1 Proposed 3D structural model for the 10 – 15 km-wide belt of transpressional
 500 deformation along the northern edge of the EPGFZ**

501 In summary, our lake studies, along with previous work, favor a model of a 10 –
 502 15 km-wide transpressional zone that deforms thick, loosely-consolidated, Miocene to re-
 503 cent clastic rocks in coastal, marine, and lake settings as illustrated in three-dimensional
 504 block diagram (Figure 10). Moving from Lake Azuey in the east to Lake Miragoâne in
 505 the west, the block diagram illustrates along-strike changes observed in the dips of the

506 thrust faults and obliquely orientation to the EPGFZ. Fold axes north of the EPGFZ range
 507 from 3 to 20 km in length, and are sigmoidally related to the EPGFZ in map view (Fig-
 508 ure 2A, B). Dip direction and amounts on these thrust faults vary from north-dipping at
 509 21° on the Jimani fault (Figure 6C and Figure 10), south-dipping on the Lamentine fault
 510 [Saint Fleur et al., 2015] at 40° , north-dipping at 70° on the Léogâne fault active during
 511 the 2010 earthquake (A–A' in Figure 3, Figure 10), and south-dipping on the Trois Baies
 512 fault at 45° (Figure 10).

513 South of the EPGFZ, transpressional folding in more rigid Cretaceous basalts and
 514 overlying Eocene limestone have broader folding wavelengths from 1 to 8 km and a weak
 515 seismogenic deformation. On the other hand, InSAR images of the 2010 earthquake indi-
 516 cate smaller folds and more seismogenic deformation in the 10 – 15 km belt north of the
 517 EPGFZ. This contrast is likely related to rock type with poorly consolidated sedimentary
 518 rocks up to several kilometers north of the EPGFZ and more consolidated carbonate rocks
 519 and basalts exposed in the highlands south of the EPGFZ [Mann et al., 1991] (Figure 2).

520 We propose that the folds north of the EPGFZ formed originally as conjugate thrust
 521 faults, reflecting the northeast to southwest convergence indicated by GPS vectors and
 522 highly transpressional character of the EPGFZ [Calais et al., 2010]. Conjugate thrust faults
 523 are common in thick, clastic sedimentary basins undergoing active, sub-horizontal short-
 524 ening [Sibson, 2012], as documented in the M_w 7.6 Chi-Chi Taiwan earthquake in 1999
 525 [Chen et al., 2002] or the M_w 7.1 Kumamoto Japan earthquake in 2016 [Lin and Chiba,
 526 2017]. Aftershocks north of the EPGFZ reflect the most recent phase of NE-SW shorten-
 527 ing on the 70° dipping reverse fault planes [Nettles and Hjörleifsdóttir, 2010], along the
 528 deeply buried Léogâne thrust fault, as shown in the cross-section of A–A' in Figure 3.

529 **6.2 Analogy between the 2010 coseismic transpressional deformation in Haiti and 530 the 1989 Loma Prieta earthquake in northern California**

531 A similar pattern of transpression in a restraining bend setting to Haiti has been de-
 532 scribed for 1989 M_w 6.9 Loma Prieta earthquake [Marshall et al., 1991] (Figure 11). The
 533 selected GPS vectors relative to a fixed North America plate [UNAVCO (*University Navstar
 534 Consortium*), 2009] indicate the transpressional setting in a gentle restraining bend setting.
 535 In the inset map of Figure 11, the 1989 hypocentral area [Marshall et al., 1991] shows
 536 the steep ($\sim 61^\circ$) dip of oblique-reverse faults of the collective Sargent and San Andreas

537 faults. Also, the 1989 coseismic elevation uplifted 0.55 m on the southwestern hanging
 538 wall of the San Andreas and Sargent faults, and subsided 0.1 m on the northeastern foot-
 539 wall block [Marshall *et al.*, 1991]. The thrusting was blind with the M_w 7.1 earthquake
 540 not being accompanied by coseismic, surface breaks. These aftershocks define a conjugate
 541 pair of reverse faults with the dominant motion on the south-dipping fault plane.

542 As in the 2010 M_w 7.0 Haiti earthquake, a secondary, blind thrust fault [Olson,
 543 1990] beneath the surface trace of the Sargent fault that, and oblique to the main San An-
 544 dreas strike-slip fault (shown in inset map of Figure 11), played a major role in the 1989
 545 fault rupture and resulting pattern of regional uplift shown in red color to the southwest
 546 and regional subsidence shown in blue color to the northeast (Figure 11).

547 While the oblique thrust planes form smaller fault segments ranging in length from
 548 3 to 11 km (Figure 2A), the 2010 earthquake demonstrates that oblique thrusts like the
 549 Léogâne fault are capable of producing a M_w 7.0 earthquake with devastating results, es-
 550 pecially when coupled with inadequate construction practices [Symithe and Calais, 2016].
 551 Paleoseismic estimates of the age of the most recent deformation of Lake Azuey, eastern
 552 Haiti, suggests that the latest activity of the EPGFZ in this area was in 1751 [Prentice
 553 *et al.*, 2010; Bakun *et al.*, 2012]. Similar analysis indicates that the latest earthquake event
 554 in the Lake Miragoâne area, western Haiti, was in 1770 [Bakun *et al.*, 2012]. This, agree-
 555 ing the previous study by Bakun *et al.* [2012], suggest the earthquake recurrence cycle
 556 along the EPGFZ is about 250 years. Therefore, in this transpressional setting, the earth-
 557 quake cycle may consist of an interplay between ruptures on the EPGFZ and ruptures on
 558 the oblique thrusts and related folds.

559 The 2010 M_w 7.0 earthquake released part of the stress of the region, but as the
 560 oblique thrusts may not be directly linked to the EPGFZ, it is possible that stresses on the
 561 EPGFZ have continued to accumulate since the 18th century [Prentice *et al.*, 2010]. Inte-
 562 grated paleoseismic study of the EPGFZ with the commonly buried oblique thrust faults,
 563 using geophysical and geologic methods, can help to inform the critical social issue of
 564 how future earthquakes will be partitioned between the larger EPGFZ and other more ob-
 565 scure, oblique faults

566 7 Conclusions

567 The main conclusions of the study are as follows:

568 1. High-resolution sonar data from two Haitian lakes that straddle the EPGFZ and
569 its northern flank demonstrates the presence of a 10 – 15 km-wide, 120 km-long, late
570 Holocene, fold-and-thrust belt, which is deforming both the clastic lowland basins along
571 the northern edge of the EPGFZ and the steep topographic highlands to the south.

572 2. In the eastern part of the study area, sonar results from Lake Azuey show that
573 the EPGFZ is more deeply buried and less active than the adjacent, newly discovered,
574 northwest-striking, northeast-dipping Jimani thrust fault. This structural relationship be-
575 tween the two faults is identical to the 2010 epicentral area 70 km to the west: the 2010
576 seismogenic, Léogâne blind thrust fault is northwest-to-east-striking, and the quiescent
577 fault to the south during the 2010 earthquake is the east-west-striking, sub-vertical EPGFZ.

578 3. The geographic distribution of 2010 aftershocks revealed that the seismogenic
579 motions of the Léogâne thrust fault and smaller motions on the EPGFZ terminated on a
580 similar northwest-striking fault: the submarine Trois Bains thrust fault. In the western-
581 most part of the study area, sonar results from Lake Mirogoâne show two overlapping and
582 active strands of the EPGFZ, and was instead diverted onto the Trois Bains thrust fault.

583 4. Our survey confirmed the pull-apart origin of Lake Mirogoâne and the lack of de-
584 formation on this western segment of the EPGFZ during the 2010 M_w 7.0 earthquake. In-
585 tegration of the geologic data across the study area show an alternation in dip along nine
586 northwest-striking, thrust faults at spacing of 5 to 40 km.

587 5. We interpret this zone of late Holocene deformation in clastic basins north of
588 the EPGFZ as the accommodation of transpressional strain supported by highly-oblique
589 GPS vectors across the study area. In this transpressional zone, coseismic deformation
590 alternates at recurrence intervals of centuries between oblique shortening structures, such
591 as Léogâne thrusts, Jimani thrusts, and Trois Bains thrusts, and strike-slip ruptures along
592 the narrow and well defined main trace of the EPGFZ.

593 6. Our results, including the eastward extension of the EPGFZ into Dominican Re-
594 public, support the “thick-skinned” strike-slip model along a 10-15 km-wide corridor of
595 left-lateral shearing centered on the EPGFZ as opposed to the southwestward propagation
596 of the Trans-Haitian fold-and-thrust belt proposed by *Pubellier et al.* [2000].

Acknowledgments

We would like to thank the Society of Exploration Geophysicists' Geoscientists Without Borders program for supporting this project along with our earlier shallow-geophysical imaging of the epicentral region on the Léogâne fan [Kocel *et al.*, 2016]. We also express our appreciation to Alex von Lignau (Haiti Department of Finance), Alfredo Lo Cicero (Oxfam Italia in Haiti) for financial and logistical support on Lake Azuey. Ludner Remarais, and Jean Robert Altidor of the Haiti Bureau of Mines and Energy for their assistance with fieldwork, permissions, and importation of equipment. Eric Fielding of NASA Jet Propulsion Laboratory (JPL)/Caltech for kindly providing the InSAR imagery. Roby Douilly of Purdue University for generously providing location information for aftershock data. We are grateful to Allied Geophysical Laboratories (AGL) and William Sager at University of Houston for assisting with equipment and fieldwork preparation. Last but not least, we sincerely thank Jean-Francois Ritz, an anonymous reviewer, and Marc Jolivet, Tectonics Associate Editor, for their valuable comments and suggestions to improve the quality of the paper. The chirp sonar data used in this paper are available on AGL datastation (<http://www.agl.uh.edu/resources-data.php>) or by contacting the corresponding author.

613 **References**

- 614 Bakun, W. H., C. H. Flores, and S. Uri (2012), Significant earthquakes on the Enriquillo
 615 fault system, Hispaniola, 1500–2010: Implications for seismic hazard, *Bulletin of the*
 616 *Seismological Society of America*, 102(1), 18–30.
- 617 Benford, B., C. DeMets, and E. Calais (2012), GPS estimates of microplate motions,
 618 northern Caribbean: evidence for a Hispaniola microplate and implications for earth-
 619 quake hazard, *Geophysical Journal International*, 191(2), 481–490.
- 620 Bien-Aimé Momplaisir, R. (1986), Contribution à l'étude géologique de la partie orientale
 621 du Massif de la Hotte (Presqu'île du Sud d'Haïti): Synthèse structurale des marges de
 622 la presqu'île à partir de données sismiques, *PhD thesis*, p. 210.
- 623 Bilham, R. (2010), Lessons from the Haiti earthquake, *Nature*, 463(7283), 878–879.
- 624 Bilham, R., and E. Fielding (2013), Remote sensing and the search for surface rupture,
 625 haiti 2010, *Natural hazards*, 68(1), 213–217.
- 626 Bourgueil, B., P. Andreieff, J. Lasnier, R. Gonnard, J. Le Metour, and J.-P. Rancon (1988),
 627 Synthèse géologique de la République d'Haïti, in *Technical report, Bureau des Mines et*
 628 *de l'Energie*, Haiti Port-au-Prince.
- 629 Bruña, J. G., U. S. Ten Brink, A. Carbó-Gorosabel, A. Muñoz-Martín, and M. G. Balles-
 630 teros (2009), Morphotectonics of the central Muertos thrust belt and Muertos Trough
 631 (northeastern Caribbean), *Marine geology*, 263(1), 7–33.
- 632 Calais, E., Y. Mazabraud, B. Mercier de Lépinay, P. Mann, G. Mattioli, and P. Jansma
 633 (2002), Strain partitioning and fault slip rates in the northeastern Caribbean from GPS
 634 measurements, *Geophysical Research Letters*, 29(18).
- 635 Calais, E., A. Freed, G. Mattioli, F. Amelung, S. Jónsson, P. Jansma, S.-H. Hong,
 636 T. Dixon, C. Prépetit, and R. Momplaisir (2010), Transpressional rupture of an un-
 637 mapped fault during the 2010 Haiti earthquake, *Nature Geoscience*, 3(11), 794–799.
- 638 Calais, É., S. Symithe, B. M. de Lépinay, and C. Prépetit (2016), Plate boundary segmen-
 639 tation in the northeastern Caribbean from geodetic measurements and Neogene geologi-
 640 cal observations, *Comptes Rendus Geoscience*, 348(1), 42–51.
- 641 Chen, K.-C., B.-S. Huang, J.-H. Wang, and H.-Y. Yen (2002), Conjugate thrust faulting
 642 associated with the 1999 Chi-Chi, Taiwan, earthquake sequence, *Geophysical Research*
 643 *Letters*, 29(8).

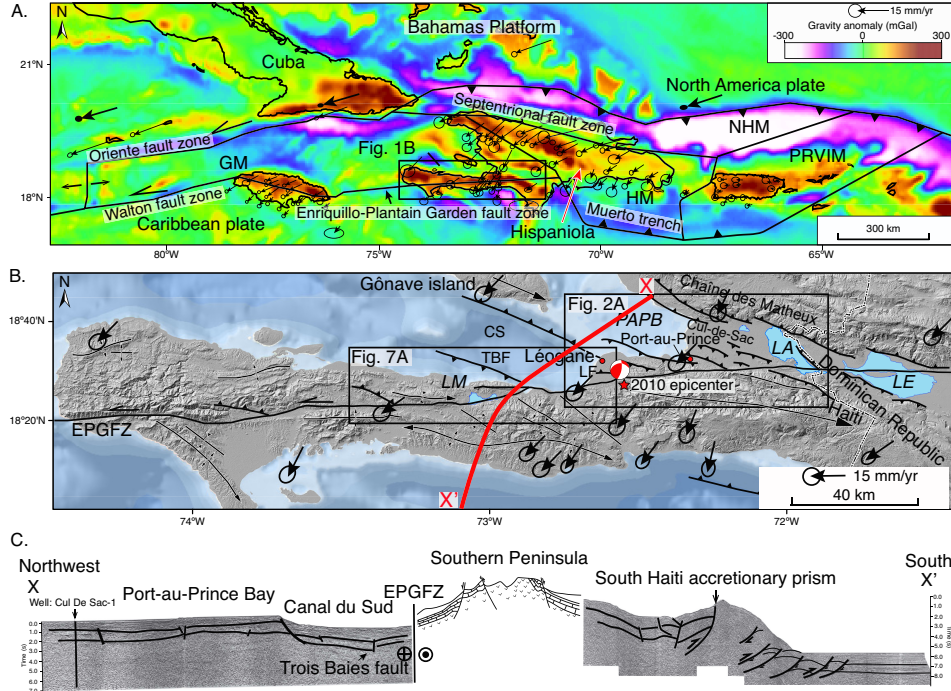
- 644 Corbeau, J., F. Rolandone, S. Leroy, B. Meyer, B. Mercier de Lépinay, N. Ellouz-
645 Zimmermann, and R. Momplaisir (2016), How transpressive is the northern Caribbean
646 plate boundary?, *Tectonics*, 35(4), 1032–1046.
- 647 Cowgill, E., T. S. Bernardin, M. E. Oskin, C. Bowles, M. B. Yıldız, O. Kreylos, A. J.
648 Elliott, S. Bishop, R. D. Gold, A. Morelan, et al. (2012), Interactive terrain visualization
649 enables virtual field work during rapid scientific response to the 2010 Haiti earthquake,
650 *Geosphere*, 8(4), 787–804.
- 651 Cox, B. R., J. Bachhuber, E. Rathje, C. M. Wood, R. Dulberg, A. Kottke, R. A. Green,
652 and S. M. Olson (2011), Shear wave velocity-and geology-based seismic microzonation
653 of Port-au-Prince, Haiti, *Earthquake Spectra*, 27(S1), S67–S92.
- 654 Dolan, J. F., H. T. Mullins, and D. J. Wald (1998), Active tectonics of the north-central
655 Caribbean: Oblique collision, strain partitioning, and opposing subducted slabs, *SPE-
656 CIAL PAPERS-GEOLOGICAL SOCIETY OF AMERICA*, pp. 1–62.
- 657 Douilly, R., J. S. Haase, W. L. Ellsworth, M.-P. Bouin, E. Calais, S. J. Symithe, J. G.
658 Armbruster, B. M. de Lépinay, A. Deschamps, S.-L. Mildor, et al. (2013), Crustal struc-
659 ture and fault geometry of the 2010 Haiti earthquake from temporary seismometer de-
660 ployments, *Bulletin of the Seismological Society of America*, 103(4), 2305–2325.
- 661 Douilly, R., H. Aochi, E. Calais, and A. Freed (2015), Three-dimensional dynamic rupture
662 simulations across interacting faults: The mw7. 0, 2010, haiti earthquake, *Journal of
663 Geophysical Research: Solid Earth*, 120(2), 1108–1128.
- 664 Fielding, E. J., A. Sladen, Z. Li, J.-P. Avouac, R. Bürgmann, and I. Ryder (2013), Kine-
665 matic fault slip evolution source models of the 2008 M7.9 Wenchuan earthquake in
666 China from SAR interferometry, GPS and teleseismic analysis and implications for
667 Longmen Shan tectonics, *Geophysical Journal International*, 194(2), 1138–1166, doi:
668 10.1093/gji/ggt155.
- 669 Frankel, A., S. Harmsen, C. Mueller, E. Calais, and J. Haase (2011), Seismic hazard maps
670 for Haiti, *Earthquake Spectra*, 27(S1), S23–S41.
- 671 Grindlay, N. R., M. Hearne, and P. Mann (2005), High risk of tsunami in the northern
672 Caribbean, *Eos, Transactions American Geophysical Union*, 86(12), 121–126.
- 673 Hashimoto, M., Y. Fukushima, and Y. Fukahata (2011), Fan-delta uplift and mountain sub-
674 sidence during the haiti 2010 earthquake, *Nature Geoscience*, 4(4), 255–259.
- 675 Hayes, G., R. Briggs, A. Sladen, E. Fielding, C. Prentice, K. Hudnut, P. Mann, F. Taylor,
676 A. Crone, R. Gold, et al. (2010), Complex rupture during the 12 January 2010 Haiti

- 677 earthquake, *Nature Geoscience*, 3(11), 800–805.
- 678 Higuera-Gundy, A., M. Brenner, D. A. Hodell, J. H. Curtis, B. W. Leyden, and M. W.
679 Binford (1999), A 10,300 14 C yr record of climate and vegetation change from Haiti,
680 *Quaternary Research*, 52(2), 159–170.
- 681 Hornbach, M. J., N. Braudy, R. W. Briggs, M.-H. Cormier, M. B. Davis, J. B. Diebold,
682 N. Dieudonne, R. Douilly, C. Frohlich, S. P. Gulick, et al. (2010), High tsunami fre-
683 quency as a result of combined strike-slip faulting and coastal landslides, *Nature Geo-
684 science*, 3(11), 783–788.
- 685 Kocel, E., R. R. Stewart, P. Mann, and L. Chang (2016), Near-surface geophysical investi-
686 gation of the 2010 Haiti earthquake epicentral area: Léogâne, Haiti, *Interpretation*, 4(1),
687 T49–T61.
- 688 Koehler, R., and P. Mann (2011), Field observations from the January 12, 2010, Haiti
689 earthquake: Implications for seismic hazards and future post-earthquake reconnaissance
690 investigations in Alaska, *Report of Investigations*, 2, 24.
- 691 Kroehler, M. E., P. Mann, A. Escalona, G. Christeson, et al. (2011), Late Cretaceous-
692 Miocene diachronous onset of back thrusting along the South Caribbean deformed belt
693 and its importance for understanding processes of arc collision and crustal growth, *Tec-
694 tonics*, 30(6).
- 695 Leroy, S., N. Ellouz-Zimmermann, J. Corbeau, F. Rolandone, B. M. Lépinay, B. Meyer,
696 R. Momplaisir, J.-L. Granja Bruña, A. Battani, C. Baurion, et al. (2015), Segmentation
697 and kinematics of the North America-Caribbean plate boundary offshore Hispaniola,
698 *Terra Nova*, 27(6), 467–478.
- 699 Lin, A., and T. Chiba (2017), Coseismic conjugate faulting structures produced by the
700 2016 m w 7.1 kumamoto earthquake, japan, *Journal of Structural Geology*, 99, 20–30.
- 701 Mann, P. (1999), Caribbean sedimentary basins: Classification and tectonic setting from
702 Jurassic to present, *Sedimentary Basins of the World*, 4, 3–31.
- 703 Mann, P., G. Draper, J. F. Lewis, et al. (1991), An overview of the geologic and tectonic
704 development of hispaniola, *Geologic and tectonic development of the North America-
705 Caribbean plate boundary in Hispaniola. Geological Society of America Special Paper*,
706 262, 1–28.
- 707 Mann, P., F. Taylor, R. L. Edwards, and T.-L. Ku (1995), Actively evolving microplate
708 formation by oblique collision and sideways motion along strike-slip faults: An example
709 from the northeastern Caribbean plate margin, *Tectonophysics*, 246(1), 1–69.

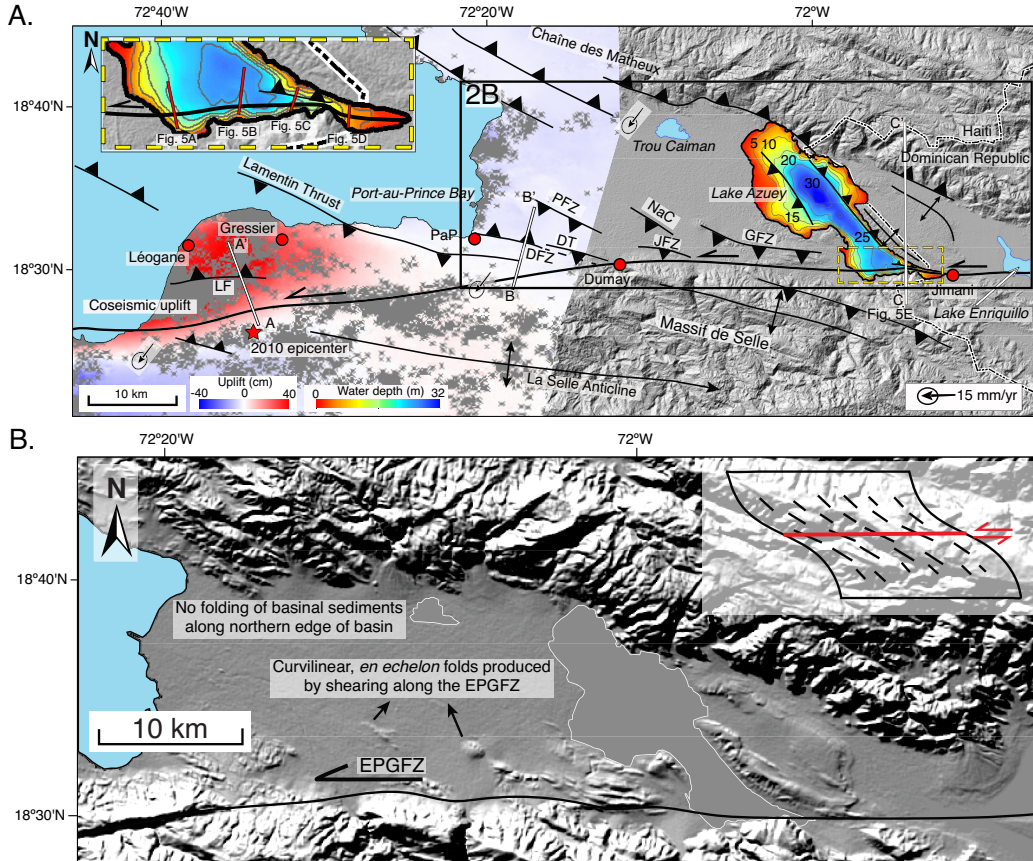
- 710 Mann, P., E. Calais, J.-C. Ruegg, C. DeMets, P. E. Jansma, and G. S. Mattioli (2002),
711 Oblique collision in the northeastern Caribbean from GPS measurements and geological
712 observations, *Tectonics*, 21(6).
- 713 Marshall, G. A., R. S. Stein, and W. Thatcher (1991), Faulting geometry and slip from co-
714 seismic elevation changes: the 18 October 1989, Loma Prieta, California, earthquake,
715 *Bulletin of the Seismological Society of America*, 81(5), 1660–1693.
- 716 Massoni, P. (1955), *Haiti: reine des Antilles*, Nouvelles Editions Latines.
- 717 McHugh, C. M., L. Seeber, N. Braudy, M.-H. Cormier, M. B. Davis, J. B. Diebold,
718 N. Dieudonne, R. Douilly, S. P. Gulick, M. J. Hornbach, et al. (2011), Offshore sedimentary effects of the 12 January 2010 Haiti earthquake, *Geology*, 39(8), 723–726.
- 720 Mercier de Lépinay, B., A. Deschamps, F. Klingelhoefer, Y. Mazabraud, B. Delouis,
721 V. Clouard, Y. Hello, J. Crozon, B. Marcaillou, D. Graindorge, et al. (2011), The 2010
722 Haiti earthquake: A complex fault pattern constrained by seismologic and tectonic ob-
723 servations, *Geophysical Research Letters*, 38(22).
- 724 Moknatian, M., M. Piasecki, and J. Gonzalez (2017), Development of Geospatial and
725 Temporal Characteristics for Hispaniola's Lake Azuei and Enriquillo Using Landsat
726 Imagery, *Remote Sensing*, 9(6), 510.
- 727 Nettles, M., and V. Hjörleifsdóttir (2010), Earthquake source parameters for the 2010 Jan-
728 uary Haiti main shock and aftershock sequence, *Geophysical Journal International*,
729 183(1), 375–380.
- 730 Odonne, F., and P. Vialon (1983), Analogue models of folds above a wrench fault,
731 *Tectonophysics*, 99(1), 31–46.
- 732 Olson, J. A. (1990), Seismicity in the twenty years preceding the loma prieta california
733 earthquake, *Geophysical Research Letters*, 17(9), 1429–1432.
- 734 Paultre, P., É. Calais, J. Proulx, C. Prépetit, and S. Ambroise (2013), Damage to engi-
735 neered structures during the 12 January 2010, Haiti (Léogâne) earthquake, *Canadian*
736 *Journal of Civil Engineering*, 40(8), 777–790.
- 737 Piasecki, M., M. Moknatian, F. Moshary, J. Cleto, Y. Leon, J. Gonzalez, and D. Co-
738 marazamy (2016), Report: Bathymetric Survey for Lakes Azuei and Enriquillo, His-
739 paniola, *Tech. rep.*, City University of New York (CUNY).
- 740 Prentice, C., P. Mann, A. Crone, R. Gold, K. Hudnut, R. Briggs, R. Koehler, and P. Jean
741 (2010), Seismic hazard of the Enriquillo-Plantain Garden fault in Haiti inferred from
742 palaeoseismology, *Nature Geoscience*, 3(11), 789–793.

- 743 Prentice, C. S., P. Mann, F. Taylor, G. Burr, and S. Valastro (1993), Paleoseismicity of
744 the north american-caribbean plate boundary (septentrional fault), dominican republic,
745 *Geology*, 21(1), 49–52.
- 746 Pubellier, M., A. Mauffret, S. Leroy, J. M. Vila, and H. Amilcar (2000), Plate boundary
747 readjustment in oblique convergence: Example of the Neogene of Hispaniola, Greater
748 Antilles, *Tectonics*, 19(4), 630–648.
- 749 Rathje, E., J. Bachhuber, B. Cox, J. French, R. Green, S. Olson, G. Rix, D. Wells, O. Sun-
750 car, E. Harp, et al. (2014), Geotechnical reconnaissance of the 2010 Haiti earthquake:
751 GEER (Geotechnical Extreme Events Reconnaissance).
- 752 Rico, P. (2017), Hydrodynamic Study of Lake Enriquillo in Dominican Republic, *Journal*
753 *of Geoscience and Environment Protection*, 5, 115–124.
- 754 Rios, J., C. McHugh, M. Hornbach, P. Mann, V. Wright, and D. Gurung (2013), Holocene
755 activity of the Enriquillo-Plantain Garden Fault in Lake Enriquillo derived from seismic
756 stratigraphy, in *AGU Fall Meeting Abstracts*, vol. 1, p. 2629.
- 757 Saint Fleur, N., N. Feuillet, R. Grandin, E. Jacques, J. Weil-Accardo, and Y. Klinger
758 (2015), Seismotectonics of southern Haiti: A new faulting model for the 12 January
759 2010 M7. 0 earthquake, *Geophysical Research Letters*, 42(23).
- 760 Segall, P., and M. Lisowski (1990), Surface displacements in the 1906 San Francisco and
761 1989 Loma Prieta earthquakes, *Science*, 250(4985), 1241–1244.
- 762 Sibson, R. (2012), Reverse fault rupturing: competition between non-optimal and optimal
763 fault orientations, *Geological Society, London, Special Publications*, 367(1), 39–50.
- 764 Sylvester, A. G. (1988), Strike-slip faults, *Geological Society of America Bulletin*, 100(11),
765 1666–1703.
- 766 Symithe, S., and E. Calais (2016), Present-day shortening in Southern Haiti from GPS
767 measurements and implications for seismic hazard, *Tectonophysics*, 679, 117–124.
- 768 Symithe, S. J., E. Calais, J. S. Haase, A. M. Freed, and R. Douilly (2013), Coseismic slip
769 distribution of the 2010 M 7.0 Haiti earthquake and resulting stress changes on regional
770 faults, *Bulletin of the Seismological Society of America*, 103(4), 2326–2343.
- 771 Taylor, F., P. Mann, S. Valastro Jr, and K. Burke (1985), Stratigraphy and radiocarbon
772 chronology of a subaerially exposed Holocene coral reef, Dominican Republic, *The*
773 *Journal of Geology*, 93(3), 311–332.
- 774 Terrier, M., A. Bialkowski, A. Nachbaur, C. Prépetit, and Y. Joseph (2014), Revision of
775 the geological context of the port-au-prince metropolitan area, haiti: implications for

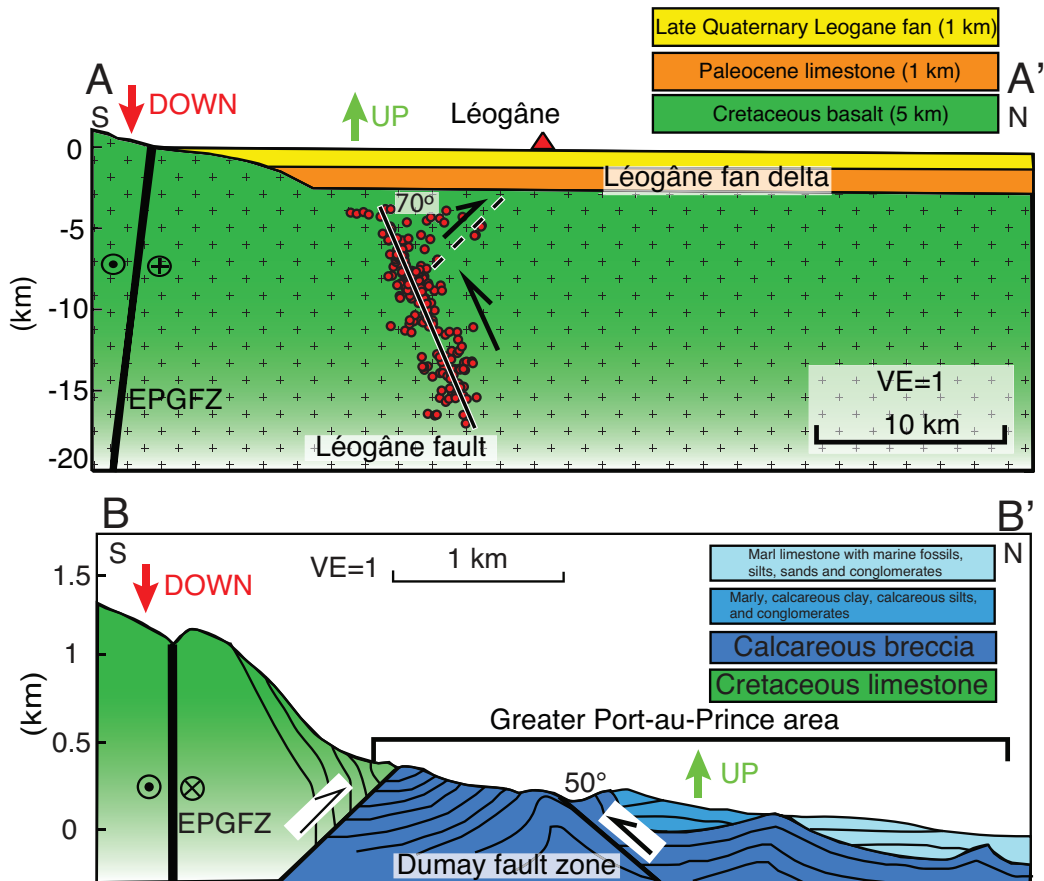
- 776 slope failures and seismic hazard assessment, *Natural Hazards and Earth System Sci-*
777 *ences, 14*(9), 2577.
- 778 UNAVCO (University Navstar Consortium) (2009), PBO GPS velocities in southern Cali-
779 fornia.
- 780 Wright, V. D., M. J. Hornbach, C. Mchugh, and P. Mann (2015), Factors contributing to
781 the 2005-present, rapid rise in lake levels, dominican republic and haiti (hispaniola),
782 *Natural Resources, 6*(08), 465.



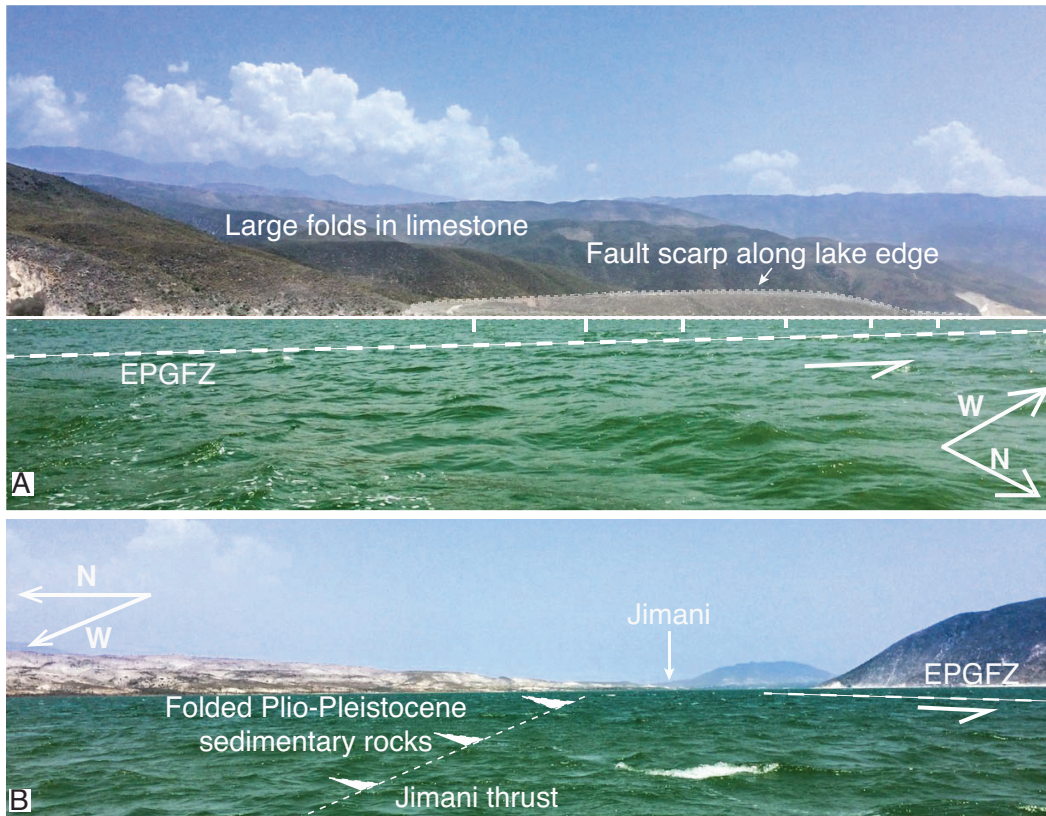
783 **Figure 1. Tectonic setting of the northeastern Caribbean and EPGFZ in southern Haiti. A:** Free-air
784 gravity anomaly map of the Greater Antilles (Cuba, Jamaica, Hispaniola, Puerto Rico) in the northeastern
785 Caribbean (<http://topex.ucsd.edu>) with gravity lows marking zones of subduction or thrusting along ma-
786 jor faults (black lines) of the North America-Caribbean plate boundary. Arrows with error ellipses from
787 *Calais et al.* [2010] are GPS vectors showing the direction and velocity of the large North American plate,
788 the Bahamas platform (**BP**), and intervening microplates relative to a fixed Caribbean plate. Microplates
789 with variable relative motions occupy the 200 km-wide plate boundary zone and include: **NHM** = North His-
790 paniola microplate; **HM** = Hispaniola microplate; **GM** = Gonâve microplate; **PRVIM** = Puerto Rico-Virgin
791 Islands microplate. Box shows more detailed map of the EPGFZ shown in B. **B:** Regional structure map of
792 the southern peninsula of Haiti with the active, left-lateral Enriquillo-Plantain Garden fault zone (EPGFZ)
793 from the Lake Enriquillo in the east to the western tip of the southern peninsula. The centroid moment tensor
794 (CMT) mechanism is from *Douilly et al.* [2013]. From east to west, key lakes and marine embayments aligned
795 parallel and overlying the EPGFZ include: **LE** = Lake Enriquillo, Dominican Republic; **LA** = Lake Azuey,
796 Haiti; **PAPB** = Port-au-Prince Bay; **CS** = Canal du Sud; and **LM** = Lake Miragoâne; **LF** = Léogâne fault.
797 Boxes shows more detailed maps of the structure of the EPGFZ and its secondary faults shown in Figure 2A
798 and Figure 7A. **C:** Composite, multichannel seismic reflection line (acquired by Canadian Superior Energy
799 Inc.) located as the red line X-X' in B that shows an unfolded area of high-angle faults in the Canal du Sud
800 tied to the offshore Cul-de-Sac-1 well, the TBFZ, the EPGFZ, the anticlinal structure of the southern penin-
801 sula, and a large, south-verging accretionary prism along the south coast of the southern peninsula. The depth
802 scale for this section is in two-way, travel time.



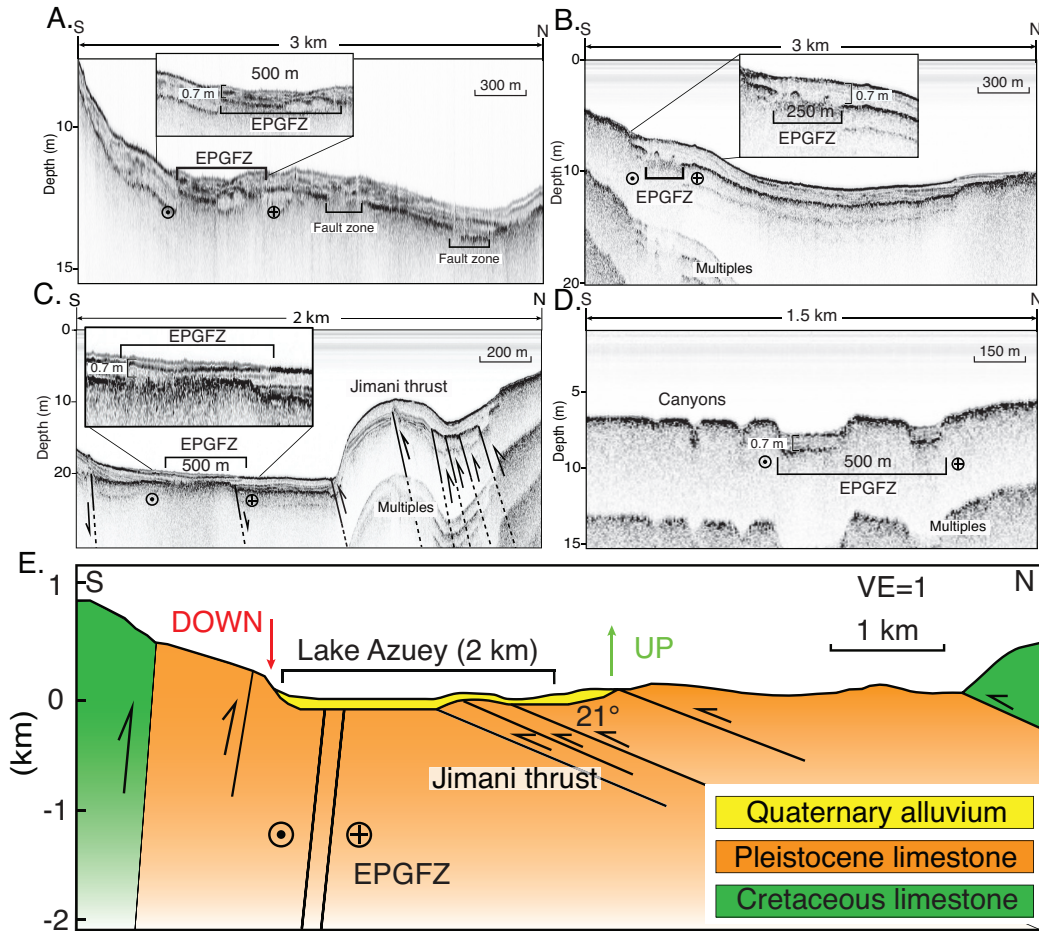
803 **Figure 2. Structure of the EPGFZ in eastern Haiti. A:** Geologic faults and folds along a 15 km-wide
 804 corridor parallel to the EPGFZ superimposed on a modified DEM and InSAR surface deformation map
 805 (courtesy of Eric Fielding at JPL) [Hayes *et al.*, 2010]. Chirp bathymetry of the Lake Azuey is also shown.
 806 GPS vectors are from *Calais et al.* [2010]. **PFZ** = Port-au-Prince fault zone; **DFZ** = Dumay fault zone; **DT**
 807 = Dumay thrust; **NaC** = Nan Cadastre thrust; **JFZ** = Jacquet fault zone; **GFZ** = Ganthier fault zone; **LF** =
 808 Léogâne fault. Line A – A': Cross-section along the blind Léogâne thrust fault (shown in Figure 3); Line B
 809 – B': Cross-section of north Port-au-Prince urban area (shown in Figure 3). **B:** Shaded DEM of the northern
 810 deformed belt in the Cul-de-Sac basin with illumination from the Figure 2A showing *en echelon* and curvi-
 811 linear folds striking west-northwest obliquely with respect to the EPGFZ and plunging beneath undeformed
 812 sediments occupying the center of the Cul-de-Sac Valley. The inserted schematic diagram is from *Odonne*
 813 and *Vialon* [1983]



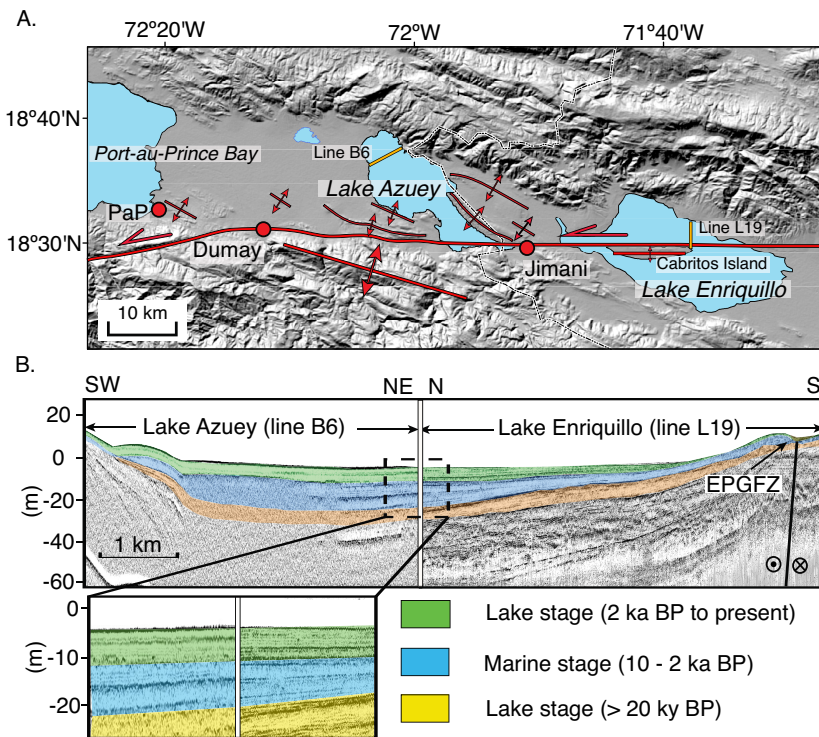
814 **Figure 3. Style of late Neogene deformation in the northern belt along three transects shown in Fig-**
 815 **ure 2. A-A':** Aftershocks of the 2010 earthquake [Douilly *et al.*, 2013, 2015] along the blind Léogâne thrust
 816 fault reveals conjugate reverse faults with the dominant slip occurring on the north-dipping fault. The red tri-
 817 angle indicates Léogâne city. **B-B':** Cross section based on surface mapping [Massoni, 1955; Cox *et al.*, 2011;
 818 McHugh *et al.*, 2011; Saint Fleur *et al.*, 2015] showing north- and south-dipping reverse faults deforming
 819 Plio-Pleistocene sedimentary rocks.



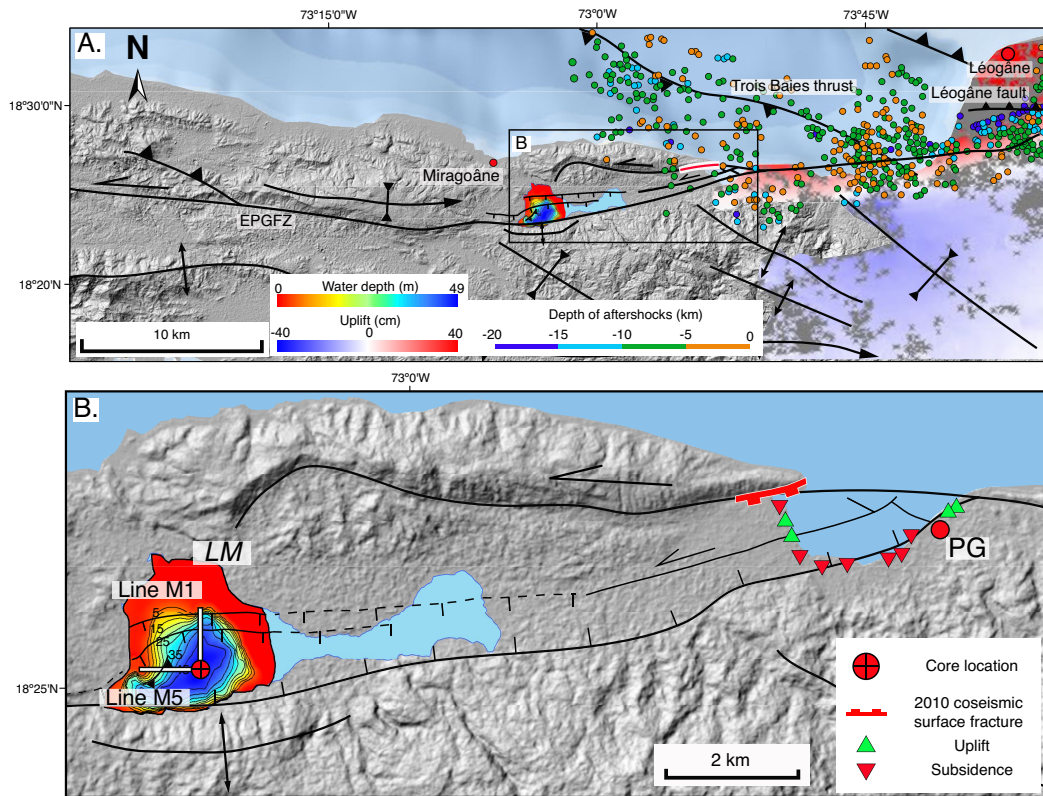
820 **Figure 4. Structure of the EPGFZ in eastern Haiti and western-most Dominican Republic. A:** Struc-
 821 tural map of Lakes Azuey (surface 15 m ASL) and Lake Enriquillo (surface 46 m BSL) are presently sepa-
 822 rated by a shallow sill 30 m ASL in the isthmus near the town of Jimani. **B:** Comparison of two Chirp lines
 823 from Lake Enriquillo by *Rios et al.* [2013] (3 km-long Line L19) and from our study of Lake Azuey (4 km-
 824 long Line B6). Identical sequences present on both lines suggest that the two lakes were once part of a single
 825 lake that has been recently separated by crustal movements related to the EPGFZ near the Jimani area. Ages
 826 of units are known from Lake Enriquillo through both exposures around the sub-sea level lake and from
 827 coring by *Rios et al.* [2013].



828 **Figure 5. Geologic setting of Lake Azuey, Haiti.** **A:** To the south, the green brackish waters of Lake
 829 Azuey are bound by the EPGFZ which forms a sharp boundary with 2 km-high, folded limestone of Paleo-
 830 gene age that forms the smooth surfaces on the skyline. One scarp is present along the edge of the lake while
 831 other parallel strands of the EPGFZ are beneath the southern part of the lake as schematically shown. **B:** To
 832 the north of the lake folded, Plio-Pleistocene strata form the uplifted, 0 – 30 m-high isthmus separating the
 833 two lakes. Approximate locations of the EPGFZ and the Jimani thrust fault are shown.

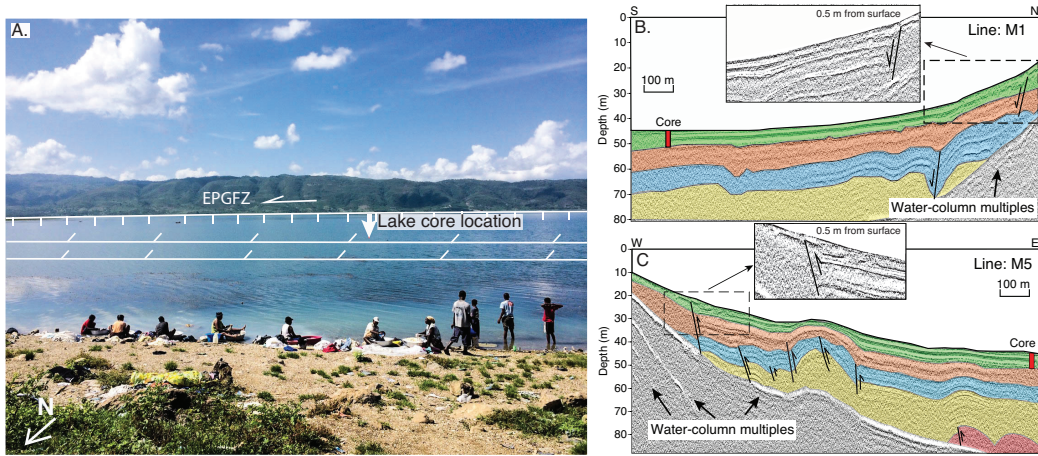


834 **Figure 6.** Chirp sonar profiles showing the relationship of the trace of the EPGFZ and a newly de-
 835 scribed thrust we have named the Jimani thrust. Cross sections of A, and B are indicated in Figure 2A.
 836 The EPGFZ beneath Lake Azuey forms a 10 m-wide zone that can be traced as a lineament to the east and
 837 west of Lake Azuey (Figure 2). The green and red horizons represent two distinguish stratigraphic layers. The
 838 two strands of the EPGFZ are buried by 0.7 m of Holocene sediment and are extrapolated to be 270 years old
 839 since their last rupture when a sedimentation rate of 2.6 mm/yr is assumed. Folds associate with the Jimani
 840 thrust are interpreted as fault propagation folds. **C:** Cross section based on both sonar survey and the surface
 841 mapping [Mann *et al.*, 1991] showing north- and south-dipping, reverse faults deforming Plio-Pleistocene
 842 sedimentary rocks.

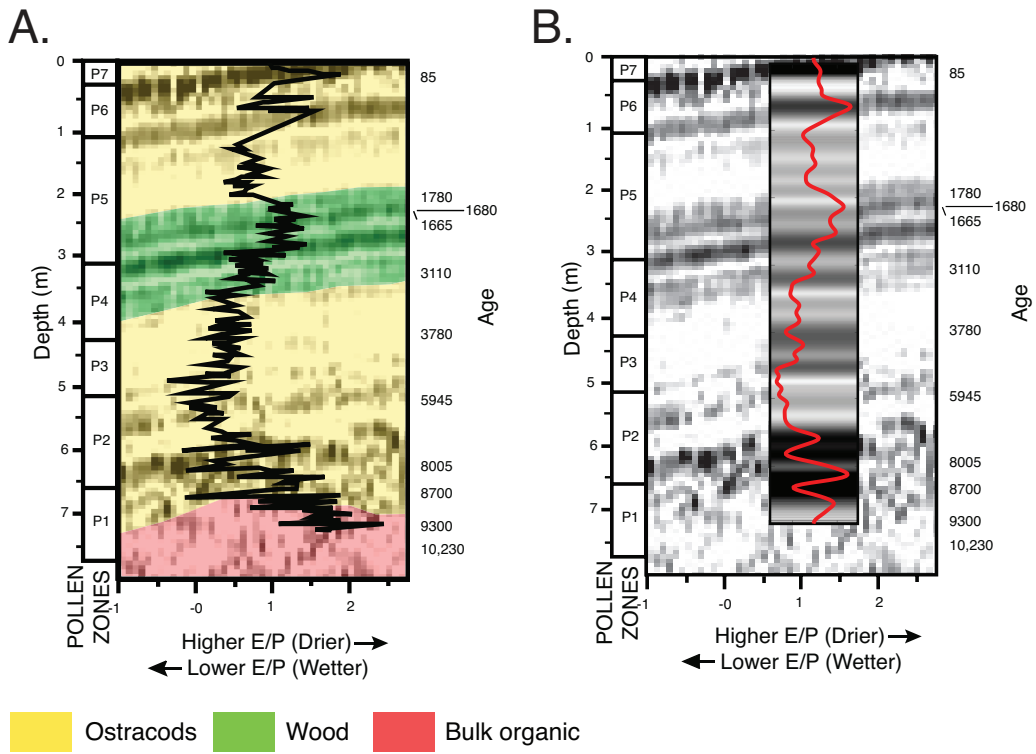


843 **Figure 7. Structure and 2010 coseismic surface deformation of the western segments of the EPGFZ.**

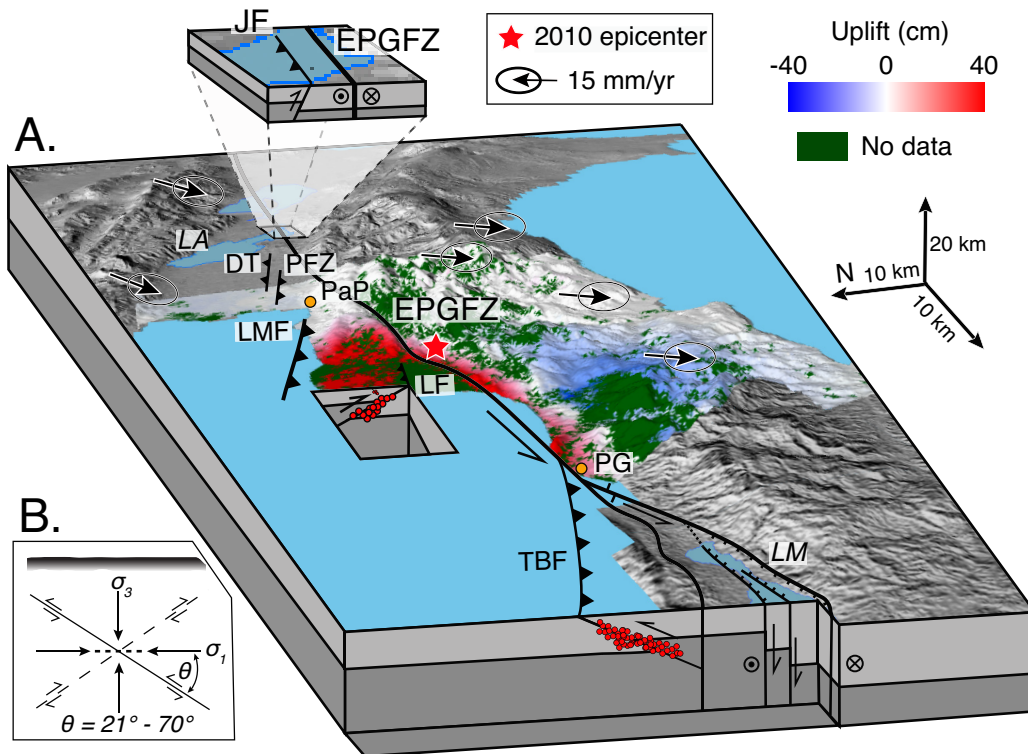
844 **A:** Structure [Prentice et al., 2010; Cowgill et al., 2012] and aftershock [Douilly et al., 2013] map of
 845 Miragoâne-Léogâne region overlain with an InSAR image (courtesy of Eric Fielding at JPL) [Hayes et al.,
 846 2010]. **B:** Zoom of the area of Petit Goâve and Lake Miragoâne showing the structure and bathymetry of the
 847 14 km², pull-apart basin mapped beneath Lake Miragoâne during this study and details of the 2010 surface
 848 fracturing and coseismic subsidence in the Petit Goâve Bay [Prentice et al., 2010]. **LM** = Lake Miragoâne;
 849 **PG** = Petit Goâve.



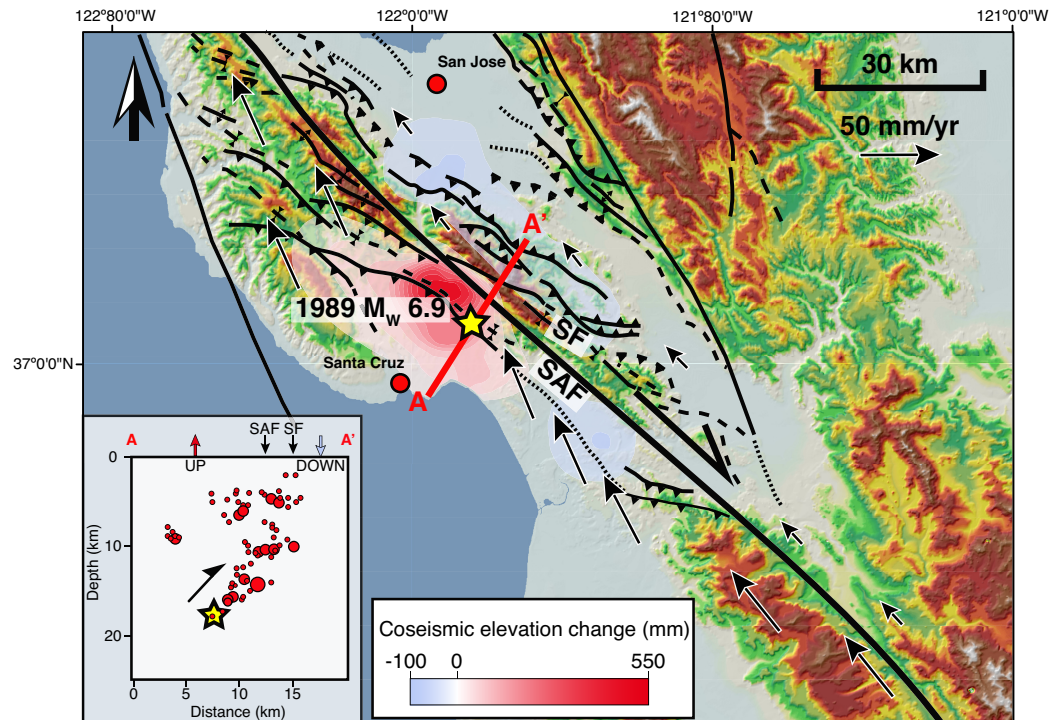
850 **Figure 8. Geologic setting and sonar profiles from Lake Miragoâne.** **A:** View looking south across the
 851 12 km-wide and 42.8 m deep, freshwater lake. The 2 km-high, ridge along the southern edge of the lake is
 852 the cumulative topographic scarp associated to the southernmost strand of the EPGFZ. The core was taken by
 853 *Higuera-Gundy et al. [1999]* and was not collected from the deepest part of the lake. **B:** North-south trending
 854 line M1 (location shown on Figure 7B). **C:** East-west trending line M5 (location shown on Figure 7B).



855 **Figure 9. Core data from Lake Miragoâne. A:** Tie between chirp sonar and core [Higuera-Gundy *et al.*,
 856 1999] extending to lacustrine sediments deformed by the EPGFZ in 1770 A.D.. **B:** Low-pass filtered E/P
 857 log (red) and the synthetic sonar profile generated from the low-pass filtered E/P log used as an acoustic
 858 impedance. The chirp sonar profiles are from the location of the red bar in the Figure 8B, C.



859 **Figure 10.** Schematic diagram of the conjugate-thrust-fault model for the 10 – 15 km-wide belt of
 860 transpressional deformation along the northern edge of the EPGFZ. **A:** Three-dimensional block diagram
 861 showing the structural, aftershocks, and the late Holocene strain partitioning in a 40-km-wide zone along a
 862 120 km-long segment of the EPGFZ. Black arrows show southwest direction of the Gonâve microplate rela-
 863 tive to the Caribbean plate [Calais *et al.*, 2010]. The 2010 InSAR-derived surface deformation map (courtesy
 864 of Eric Fielding at JPL) [Hayes *et al.*, 2010] show a large component of shortening accommodated on a 40
 865 km-wide zone of oblique thrusts and folds north of the EPGFZ. **PaP** = Port-au-Prince; **PG** = Petit Goave;
 866 **LA** = Lake Azuey; **LM** = Lake Miragoâne-Léogâne; **JF** = Jimani thrust fault; **DT** = Dumay thrust; **PFZ** =
 867 Port-au-Prince fault zone; **LMF** = Lamartin thrust fault; **TBF** = Trois Baies thrust fault; **LF** = Léogâne fault.
 868 **B:** Schematic diagram, modified from Sibson [2012], of the conjugate thrust faults.



869 **Figure 11. Structural map of the southern San Francisco Bay region, the coseismic elevation and**
 870 **the aftershock cross-section of 1989 M_w 6.9 Loma Prieta earthquake.** The selected GPS vectors relative
 871 to a fixed North America plate are from UNAVCO (*University Navstar Consortium*) [2009]. The coseismic
 872 elevation change and aftershock cross-section are modified from Marshall *et al.* [1991]. **SAF:** San Andreas
 873 **Fault; SF:** Sargent Fault.